HHS Public Access

Author manuscript

Cell Rep. Author manuscript; available in PMC 2020 August 31.

Published in final edited form as:

Cell Rep. 2020 August 11; 32(6): 108013. doi:10.1016/j.celrep.2020.108013.

Protein O-GlcNAc Modification Links Dietary and Gut Microbial Cues to the Differentiation of Enteroendocrine L Cells

Ming Zhao[1], **Kaiqun Ren**[1,2], **Xiwen Xiong**[3], **Meng Cheng**[1,8], **Zengdi Zhang**[1], **Zan Huang**[1], **Xiaonan Han**[4], **Xiaoyong Yang**[5,6], **Emilyn U. Alejandro**[1], **Hai-Bin Ruan**[1,7,*]

[1]Department of Integrative Biology and Physiology, University of Minnesota Medical School, Minneapolis, MN 55455, USA

[2]College of Medicine, Hunan Normal University, Changsha, Hunan 410013, China

[3]School of Forensic Medicine, Xinxiang Medical University, Xinxiang, Henan 453003, China

[4]Division of Gastroenterology, Hepatology, and Nutrition, Cincinnati Children's Hospital Medical Center, Cincinnati, OH 45229, USA

[5]Department of Cellular and Molecular Physiology, Yale University School of Medicine, New Haven, CT 06519, USA

[6]Program in Integrative Cell Signaling and Neurobiology of Metabolism, Department of Comparative Medicine, Yale University School of Medicine, New Haven, CT 06519, USA

[7]Center for Immunology, University of Minnesota Medical School, Minneapolis, MN 55455, USA

[8]Present address: Curriculum in Genetics and Molecular Biology, Lineberger Comprehensive Cancer Center, University of North Carolina at Chapel Hill, Chapel Hill, NC 27599, USA

SUMMARY

Intestinal L cells regulate a wide range of metabolic processes, and L-cell dysfunction has been implicated in the pathogenesis of obesity and diabetes. However, it is incompletely understood how luminal signals are integrated to control the development of L cells. Here we show that food availability and gut microbiota-produced short-chain fatty acids control the posttranslational modification on intracellular proteins by O-linked β-N-acetylglucosamine (O-GlcNAc) in intestinal epithelial cells. Via FOXO1 O-GlcNAcylation, O-GlcNAc transferase (OGT) suppresses expression of the lineage-specifying transcription factor Neurogenin 3 and, thus, L cell differentiation from enteroendocrine progenitors. Intestinal epithelial ablation of OGT in mice not only causes L cell hyperplasia and increased secretion of glucagon-like peptide 1 (GLP-1) but also

*Correspondence: hruan@umn.edu.

AUTHOR CONTRIBUTIONS

M.Z. designed, performed, and analyzed most experiments. K.R., X.X., M.C., and X.H. assisted with histology, western blotting, and qPCR. Z.Z. and Z.H. constructed plasmids. X.Y. generated the *Rosa26-rOGT-floxed* mice. E.U.A. assisted with generating the *Ngn3-Ogt* KO mice. H.-B.R. conceived, designed, and performed experiments. M.Z. and H.-B.R. wrote the manuscript.

SUPPLEMENTAL INFORMATION

Supplemental Information can be found online at https://doi.org/10.1016/j.celrep.2020.108013.

DECLARATION OF INTERESTS

The authors declare no competing interests.

disrupts gut microbial compositions, which notably contributes to decreased weight gain and improved glycemic control. Our results identify intestinal epithelial O-GlcNAc signaling as a brake on L cell development and function in response to nutritional and microbial cues.

Graphical Abstract

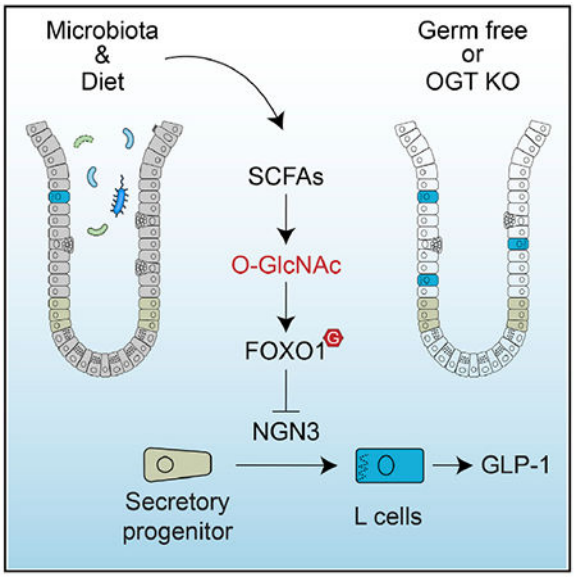

In Brief

Zhao et al. identify OGT in intestinal epithelial cells as a “molecular brake” on L cell development and function in response to nutritional and microbial cues. OGT inhibits *Ngn3* gene transcription and enteroendocrine differentiation via FOXO1 O-GlcNAcylation. Microbiota-derived SCFAs drive epithelial O-GlcNAcylation, which further influences gut microbiota to control systemic metabolism.

INTRODUCTION

Enteroendocrine cells (EECs) are specialized epithelial cells of the gastrointestinal tract that form the largest endocrine system in the body. By sensing luminal signals, EECs produce and secret neurotransmitters and hormones to modulate a variety of metabolic functions locally and systemically, such as gut motility, nutrient intake and absorption, glucose metabolism, lipid homeostasis, and energy balance (Mellitzer et al., 2010; Moran-Ramos et al., 2012; Holst, 2013; Gribble and Reimann, 2016). Studies suggest that defects in EEC function and gut hormone secretion are associated with human obesity and diabetes (Toft-Nielsen et al., 2001; Vilsbøll et al., 2001; Faerch et al., 2015). Therefore, gut hormones are excellent therapeutic candidates for treatment of metabolic diseases. Agonists of the glucagonlike peptide 1 (GLP-1) receptor and inhibitors of dipeptidyl peptidase-4 (DPP4), which inactivates GLP-1, are widely used for effective glycemic control in diabetic patients, with demonstrated benefits of weight loss and cardioprotection as well (Cantini et al., 2016; Drucker, 2016). The gut hormone responses to bariatric procedures have been proposed to be a mechanism for weight loss and improvement in glucose metabolism after surgery

(Hutch and Sandoval, 2017). Moreover, dual and triple gut hormone receptor agonists are considered next-generation therapies for metabolic diseases (Troke et al., 2014; Brandt et al., 2018). Despite extensive application of enteroendocrine hormones in the clinic, the pathophysiological regulation of EEC development and function is incompletely understood, and direct means to modulate EEC differentiation *in vivo* are still largely lacking.

Traditionally, EECs are classified on the basis of the hormones they produce: L cells (GLP-1 and peptide YY [PYY]), K cells (gastric inhibitory polypeptide [GIP]), I cells (cholecystokinin [CCK]), D cells (somatostatin [SST]), S cells (secretin [SCT]), and enterochromaffin (EC) cells (serotonin [5-HT]) (Latorre et al., 2016). However, substantial data from recent studies using transcriptional profiling, transgenic reporter lines, immunohistochemistry, and particularly single-cell RNA sequencing have demonstrated that there is significant coexpression of hormones and crossover between EEC subtypes (Egerod et al., 2012; Habib et al., 2012; Gribble and Reimann, 2016; Haber et al., 2017; Gehart et al., 2019). EECs differentiate from the common $LGR5^+$ pluripotent stem cells in the base of the crypt compartment (Cheng and Leblond, 1974; Barker et al., 2007). Three basic helix-loop-helix transcription factors, including ATOH1, Neurogenin 3 (encoded by the *Ngn3* gene), and NeuroD1, are expressed sequentially and function in cascades for EEC differentiation (Schonhoff et al., 2004a). ATOH1 is critical for development of all three secretory cell types (Yang et al., 2001; Shroyer et al., 2007), whereas Neurogenin 3 is specific for determination and differentiation into EECs (Jenny et al., 2002; Lee et al.,2002; Mellitzer et al., 2010). NeuroD1, a downstream target of Neurogenin 3, is important for S and I cell differentiation (Mutoh et al., 1997; Naya et al., 1997). In addition, PAX4 and PAX6 have been shown to control L, K, D, and EC cell differentiation (Larsson et al., 1998). Recently, novel general and lineage-specific regulators of EEC differentiation have also been identified by real-time single-cell transcriptional profiling (Gehart et al., 2019). Nonetheless, the upstream molecular mechanisms fine-tuning the transcriptional machinery for EEC development have not been fully elucidated.

Within the last three decades, it was discovered that thousands of cytoplasmic and nuclear proteins are modified by a single O-linked β-N-acetylglucosamine (O-GlcNAc) moiety at serine or threonine residues, termed O-GlcNAcylation (Torres and Hart, 1984; Hart et al., 2007, 2011). O-GlcNAcylation is radically different from other types of glycosylation and, analogous to phosphorylation, plays a central role in signaling pathways relevant to normal cell physiology and chronic human diseases, including cardiovascular disease, diabetes, neurodegeneration, and cancer (Bond and Hanover, 2013; Ruan et al., 2013b; Yang and Qian, 2017). The enzymes O-GlcNAc transferase (OGT) and O-GlcNAcase (OGA) mediate addition and removal of O-GlcNAc, respectively (Vocadlo, 2012; Joiner et al., 2019). O-GlcNAc signaling acts as a hormone and nutrient sensor to control many biological processes, such as gene transcription, translation, protein stability and folding, and cell signaling (Hanover et al., 2012; Ruan et al., 2012, 2013a, 2014, 2017; Liu et al., 2019). Recently, we found that, in the intestinal epithelium, levels of protein O-GlcNAcylation are reduced in patients with inflammatory bowel disease and showed that OGT is required for survival of intestinal epithelial cells and their interplay with gut microbiota (Zhao et al., 2018). Here we further determined that intestinal epithelial O-GlcNAcylation is sensitive to

microbiota-derived short-chain fatty acids, controls EEC lineage differentiation and function, and regulates systemic energy and glucose metabolism.

RESULTS

Deficiency in Intestinal Epithelial OGT Promotes L Cell Differentiation and Metabolic Health in Mice

To determine whether protein O-GlcNAcylation negatively controls EEC development, we genetically deleted OGT specifically in intestinal epithelial cells (*Vil-Ogt* knockout [KO]) by crossing the *Villin-Cre* and *Ogt-floxed* mouse lines (Ruan et al., 2014; Zhao et al., 2018). The *Ogt* gene is located on the X chromosome; thus, male mice are hemizygous. Levels of *Ngn3* and various gut hormone genes, including *Gcg* (L cells), *Gip* (K cells), and *Cck* (I cells), were elevated in the ileum and colon of *Vil-Ogt* KO males compared with littermate controls (Figures 1A and 1B). Segment-specific changes were also observed. For example, *Pax6* and the EC cell marker *Chga* were only increased in the *Vil-Ogt* KO ileum (Figure 1A). Expression of the L cell-specific regulator *Hoxb9* and the hormone *Pyy* was upregulated in the colon of *Vil-Ogt* KO mice (Figure 1B). We then specifically examined L cells and found that GLP-1^+ and PYY^+ cell numbers in the intestine (Figures 1C–1E) and GLP-1 levels in the serum (Figure 1F) were increased in *Vil-Ogt* KO males.

Concomitantly, hemizygous *Vil-Ogt* KO male mice showed lower body weight (Figure 2A), less fat and lean mass (Figure 2B), decreased random blood glucose (Figure 2C), and enhanced glucose clearance rate during an oral glucose tolerance test (Figures 2D and 2E) compared with littermate control males. Similarly, homozygous *Vil-Ogt* KO females also had decreased body weight (Figure 2F) and improved glucose tolerance (Figures 2G and 2H). Collectively, these data demonstrate that OGT deficiency in the intestinal epithelium promotes enteroendocrine L cell development and improves body weight and glucose metabolism.

A Cell-Autonomous Action of O-GlcNAcylation on L Cell Development

Vil-Ogt KO mice develop intestinal damage and inflammation (Zhao et al., 2018), which may confound our findings regarding L cell development. We then performed *ex vivo* intestinal organoid culture and found that OGT inhibition by OSMI-1 decreased global protein O-GlcNAcylation (Ortiz-Meoz et al., 2015; Figure S1A); increased the expression of *Ngn3, Hoxb9,* and the L cell hormone genes *Gcg* and *Pyy* (Figure 3A); and notably enhanced GLP-1 secretion from organoids (Figure 3B).

To extend these findings *in vivo*, we then specifically overexpressed OGT in intestinal epithelial cells by crossing *Villin-Cre* with a mouse line harboring an inducible rat OGT transgene in the *Rosa26* locus (Yang et al., 2020; Figure 3C). qRT-PCR showed that expression of the rat *Ogt* gene was significantly up-regulated in intestinal tissues (Figure 3D). Immunoblotting further confirmed OGT overexpression and elevation of global protein O-GlcNAcylation (Figure 3E). Inflammatory gene expression and intestinal epithelial permeability were comparable in control and *Vil-*Cre^+*;R26-rOGT* mice (Figures S1B–S1D), suggesting that OGT overexpression did not overtly cause epithelial damage or

inflammation. As expected, *Vil-Cre*$^{+}$*;R26-rOGT* mice displayed reduced L cell numbers in the colon (Figures 3F and 3G) and GLP-1 levels in the serum (Figure 3H) compared with controls. Although similar body weight (Figure 3I) and fasting glucose levels (Figure 3J) were observed in controls and *Vil-Cre*$^{+}$*;R26-rOGT* mice, *Vil-Cre*$^{+}$*;R26-rOGT* mice had higher fasting insulin levels in the blood (Figure 3K) and showed a trending increase in homeostatic model assessment of insulin resistance (HOMA-IR, Figure 3L). These results demonstrate that OGT and protein O-GlcNAcylation negatively regulate L cell development and glucose metabolism in a cell-autonomous manner.

OGT Suppresses *Ngn3* Gene Transcription via FOXO1 O-GlcNAcylation

NGN3 plays a pivotal role in controlling the commitment of pluripotent progenitor cells toward the EEC lineage (Jenny et al., 2002; Mellitzer et al., 2010). We could not detect O-GlcNAcylation of overexpressed NGN3 (Figure S2A); thus we sought to test whether OGT controls *Ngn3* gene transcription. Consistent with the observation that the expression of *Ngn3* and its downstream genes was upregulated in *Vil-Ogt* KO intestine (Figures 1A and 1B), OGT was able to suppress *Ngn3* promoter activity in cultured cells (Figure 4A). Previous reports have shown that FOXO1, an O-GlcNAc-modified protein, negatively regulates *Ngn3* transcription (Al-Masri et al., 2010; Bouchi et al., 2014). We sought to test whether OGT represses *Ngn3* transcription via FOXO1 O-GlcNAcylation. Consistent with previous reports (Housley et al., 2008; Fardini et al., 2014), we found that OGT overexpression (Figure 4B) and specific inhibition of OGA by 6-Ac-CAS (Figure 4C) substantially increased FOXO1's transactivation activity on insulin-responsive elements. We then mutated four known O-GlcNAc sites on FOXO1 (T314, S547, T645, and S651) to alanine (FOXO1-4A) (Housley et al., 2008). FOXO1-4A showed impairment in O-GlcNAcylation compared with wild-type FOXO1, particularly when OGA was inhibited by PUGNAc (Figure 4D). As a result, the 4A mutation diminished the transcriptional activator function of FOXO1 when co-expressed with OGT (Figure 4E).

On the other hand, FOXO1 acted as a transcriptional repressor on the *Ngn3* promoter (Figure 4F), and such inhibitory activity was absent when FOXO1 O-GlcNAcylation was ablated (Figure 4F). To test whether the effect of OGT on L cell development is dependent on FOXO1, we treated ileal organoids with the OGT inhibitor OSMI-1 in the presence or absence of a FOXO1 inhibitor, AS1842856. Regarding FOXO1's positive target genes, such as *Gopc,* suppression oi transcription by OSMI-1 was abolished when AS1842856 was present (Figure S2B). Notably, the ability of OGT inhibition by OSMI-1 to promote expression of *Ngn3, Gcg,* and *Pyy* genes (Figure 4G–I) and secretion of GLP-1 (Figure 4J) was diminished when the transcriptional activity of FOXO1 was blocked by AS1842856. Together, these results suggest that FOXO1 O-GlcNAcylation mediates the transcriptional suppression of the *Ngn3* gene by OGT.

OGT in the *Ngn3* Lineage Controls Differentiation of L Cells

Next we sought to determine whether O-GlcNAc signaling in *Ngn3*$^{+}$ progenitors controls L cell differentiation. To do so, we generated EEC-specific OGT KO mice using the *Ngn3-Cre* line (Schonhoff et al., 2004b). No changes in body weight were observed between wild-type and *Ngn3-Ogt* KO mice (Figure 5A). Pancreatic endocrine progenitors also express *Ngn3,*

and deletion of OGT in islet progenitors (E.U.A., unpublished data) or insulin$^+$ cells (Alejandro et al., 2015) induces diabetes as a result of β-cell dysfunction as early as 4 weeks of age (Figures 5B and S3A). Therefore, we analyzed *Ngn3-Ogt* KO mice before weaning, when they had similar body weight, slightly lower blood glucose (Figure 5A, B), and normal β-cell mass in *Ngn3-Ogt* KO compared with littermate controls (E.U.A., unpublished data). Immunostaining showed that GLP-1$^+$ and PYY$^+$ L cells (Figures 5C and 5D) and ChgA$^+$ EC cells (Figures S3B and S3C) modestly increased their numbers in the *Ngn3-Ogt* KO intestine. At this age, when assessed for oral glucose tolerance, *Ngn3-Ogt* KO mice had higher initial blood glucose levels, probably because of defects in β-cells, but faster glucose clearance, which could be attributed to GLP-1-mediated insulin hypersensitivity (Figure 5E).

To eliminate potential confounding effects from *Ngn3*-expressing pancreas and neurons, we isolated and cultured ileal organoids from control and *Ngn3-Ogt* KO mice to assess L cell development. qPCR revealed no changes in the expression of markers for enterocytes (*Slc5a1*), goblet cells (*Muc2*), Paneth cells (*Defa6*), or tuft cells (*Dclk1*) (Figure S3D). Among EEC marker genes, L cell-specific *Hoxb9, Gcg,* and *Pyy* were significantly upregulated in *Ngn3-Ogt* KO organoids, whereas *Ngn3* and genes encoding other EEC hormones were unaffected (Figures 5F and S3E). As a result, more GLP-1 peptides could be detected in the medium of *Ngn3-Ogt* KO organoids than in a wild-type culture (Figure 5G). OGT inhibition by OSMI-1 and *Ngn3-Ogt* KO significantly increased the number of GLP-1$^+$ cells (Figures 5H and 4I; Table S1). However, OSMI-1 could not further promote L cell hyperplasia in *Ngn3-Ogt* KO organoids (Figures 5H and 5I), suggesting that OSMI-1 acted on *Ngn3*$^+$ EEC progenitors to promote L cell development.

Protein O-GlcNAcylation and L Cell Function Are Inversely Regulated

Nutrients like glucose and fatty acids drive the hexosamine synthetic pathway and protein O-GlcNAcylation. We then sought to test whether levels of intestinal epithelial O-GlcNAcylation are regulated by food availability. Overnight fasting in mice significantly reduced the level of global protein O-GlcNAcylation in colonic epithelial cells, which was replenished by 4 h of refeeding (Figure 6A). In rodents, high-fat diet (HFD)-induced obesity impairs L cell function (Gil-Lozano et al., 2016; Richards et al., 2016; Zheng et al., 2017). However, we found that intestinal protein O-GlcNAcylation was substantially increased by HFD in mice (Figure 6B).

The gut microbiota has a significant effect on host metabolism, partially through synthesis of short-chain fatty acids (SCFAs) (Tremaroli and Bäckhed, 2012; Rosenbaum et al., 2015; Knip and Siljander, 2016). L cell hyperplasia was observed in germ-free (GF) and antibiotic-treated mice and could be suppressed by microbiota colonization and SCFAs (Wichmann et al., 2013; Arora et al., 2018; Zarrinpar et al., 2018). Similarly, we observed increased levels of *Gcg* and *Pyy* RNA (Figure 6C) and serum GLP-1 in GF mice (Figure 6D) compared with age-matched, conventionally housed specific pathogen-free (SPF) mice purchased from the same vendor. Immunostaining showed that global protein O-GlcNAcylation in the cytoplasm of colonocytes was dramatically inhibited in GF mice (Figures 6E and 6F). We also treated C57BL/6 mice with multiple broad-spectrum antibiotics (ampicillin, gentamicin, metronidazole, neomycin, and vancomycin) to deplete the gut microbiota by oral gavage for

2 weeks (Hill et al., 2010; Reikvam et al., 2011). 16 s rRNA sequencing of fecal DNA confirmed that antibiotic treatment significantly reduced gut microbial diversity (Figures S4A and S4B). A substantial reduction in cytoplasmic levels of colonic O-GlcNAcylation was observed by immunostaining (Figures 6G and 6H). Moreover, oral administration of a mixture of SCFAs (acetate, propionate, and butyrate) to mice largely restored the levels of O-GlcNAcylation in colonic epithelial cells (Figures 6I and S4C). In addition, in cultured human intestinal Caco-2 cells, SCFA treatment was sufficient to raise protein O-GlcNAcylation levels (Figure 6J). These data demonstrate that dietary nutrients and gut microbiota-derived SCFAs promote epithelial O-GlcNAcylation.

To test whether SCFAs suppress L cell function via O-GlcNAcylation, we treated ileal organoids with SCFAs and were able to observe repression of *Gcg* gene expression (Figure 6K) and GLP-1 secretion (Figure 6L) by SCFAs. Notably, treating cells simultaneously with the OGT inhibitor OSMI-1 could modestly reverse the repressive effect of SCFAs (Figures 6K and 6L). It is worth noting that SCFAs inhibited GLP-1 secretion in wild-type and *Ngn3-Ogt* KO organoids (Figure S4D), indicating that OGT-independent pathways may also exist. Collectively, these results established O-GlcNAcylation as a molecular link between SCFAs and L cell function.

Microbial Disruption in *Vil-Ogt* KO Mice Contributes to Metabolic Improvement

Intestinal epithelial O-GlcNAcylation not only responds to microbial cues but also modulates the gut microbiota; we recently demonstrated that OGT deficiency in intestinal epithelial cells is associated with microbial dysbiosis in mice (Zhao et al., 2018). We then sought to determine whether the microbial changes in *Vil-Ogt* KO mice contribute to the systemic improvement in metabolism through fecal microbiota transplantation (FMT; Figure S5A). Microbiota-depleted or GF mice receiving FMT from *Vil-Ogt* KO mice gained significantly less body weight compared with their counterparts receiving FMT from wild-type (WT) mice (Figures 7A and 7B). GF mice colonized with *Vil-Ogt* KO microbiota had much less fat composition (Figure 7C) and reduced white adipose tissue (WAT) weight (Figure 7D). Food intake (Figure 7E) and locomotor activity (Figure 7F) were similar in mice receiving FMT from WT and *Vil-Ogt* KO mice. Mice receiving *Vil-Ogt* KO FMT had a trending increase in respiratory exchange rate (RER; Figures 7G and 7H), suggesting that glucose was used preferentially in these mice. Moreover, total energy expenditure, determined by heat production normalized to body weight (Figure 7I) or adjusted to body weight using analysis of covariance (ANCOVA) (Figure 7J), were increased remarkably in GF mice colonized with *Vil-Ogt* KO microbiota (Tschöp et al., 2011). Intriguingly, *Vil-Ogt* KO microbiota was able to marginally increase L cell numbers in recipient mice (Figure S5B). However, no substantial differences in random blood glucose (Figure S5C), oral glucose tolerance (Figure S5D), or insulin tolerance (Figure S5E) were observed in mice receiving FMT from WT or *Vil-Ogt* KO mice. These data indicate that changes in gut microbiota associated with *Vil-Ogt* KO are sufficient to drive L cell hyperplasia and reduced weight gain but not improvement in glucose metabolism.

DISCUSSION

Enteroendocrine L cells evolve multiple sensory mechanisms to detect different classes of luminal nutrients, including carbohydrates, lipids, and proteins (Gribble and Reimann, 2016). Recently, growing evidence has demonstrated that the gut microbiota influences intestinal homeostasis, glucose metabolism, and energy balance. Here we show that microbiota-derived SCFAs drive the levels of protein O-GlcNAcylation in intestinal epithelial cells, which serve as a negative regulator of L cell development and function. Loss of intestinal epithelial OGT and protein O-GlcNAcylation in mice results in L cell hyperplasia, improved metabolism, and microbial changes that contribute to metabolic health. Mechanistically, we determined that OGT-mediated FOXO1 O-GlcNAcylation suppresses *Ngn3* gene expression and inhibits differentiation of *Ngn3*$^{+}$ EEC progenitors toward L cells *in vivo*.

In addition to aiding digestion and producing vitamins, the microbiota benefits the host through synthesis of SCFAs, including acetate, propionate, and butyrate (Tremaroli and Bäckhed, 2012). SCFAs bind to G-protein-coupled receptor 43 (GPR43, also known as free fatty acid receptor 2 [FFAR2]) and GPR41 (FFAR3) to regulate lipid and glucose metabolism (den Besten et al., 2013). Butyrate and propionate are also potent inhibitors of histone deacetylases (HDACs) (Kasubuchi et al., 2015). More importantly, SCFAs are preferred metabolic substrates for intestinal epithelial cells (den Besten et al., 2013); however, regulation of L cell development and function by SCFAs remains controversial. SCFAs have been shown to increase the number of L cells and induce PYY and GLP-1 secretion via GPR43 and GPR41 (Tolhurst et al., 2012; Petersen et al., 2014; Psichas et al., 2015). However, intestinal KO of GPR43 and GPR41 does not alter glucose tolerance in diabetic animals (Tang et al., 2015), indicating that other receptors or sensing mechanisms for SCFAs might be involved. On the other hand, we and others have shown that GLP-1 transcription and secretion are more than 2-fold higher in GF mice than in conventionally raised mice. Importantly, intestinal colonization of the gut microbiota increases SCFAs and suppresses L cell function (Wichmann et al., 2013; Arora et al., 2018). More recently, Larraufie et al. (2018) demonstrated that SCFAs, particularly propionate and butyrate, strongly increase *PYY* gene expression but slightly suppress *GCG* expression in human L cells. The reasons for these discrepancies among the reported results are still unclear but could be manifold: different assay systems used (cell lines versus organoids versus whole organisms, rodents versus humans), non-linear but biphasic responses to SCFA concentrations, shifting the differentiation of progenitors toward other EEC lineages (K, I, S, N, EC cells, etc.), divergent effects on L cells versus other mucosal cell types (Nøhr et al., 2013, 2015), and complex interplay of SCFAs with other microbiota-derived metabolites and signals. Further studies are required to fully elucidate the microbial control of L cell development and function.

A large body of literature has shown that inflammatory bowel disease (IBD), including ulcerative colitis (UC) and Crohn’s disease (CD), is generally associated with increased numbers of intestinal EECs and blood levels of gut hormones in humans (Worthington et al., 2018). These enteroendocrine responses are thought to be involved in tissue repair and responsible for the reduced appetite and altered gut mobility associated with IBD. However,

current IBD animal models that are induced by chemicals, including 2,4,6-trinitrobenzenesulfonic acid (TNBS) and dextran sulfate sodium (DSS), and genetic alterations (such as *Tcra*$^{-/-}$ and *Il2*$^{-/-}$) cannot fully recapitulate the EEC alterations found in IBD patients (Worthington et al., 2018). Our previous study has shown that levels of OGT and protein O-GlcNAcylation are reduced in inflamed intestinal epithelium in humans and that loss of intestinal epithelial OGT leads to microbial dysbiosis and intestinal inflammation in mice (Zhao et al., 2018). In this study, we further show that OGT deficiency and associated microbial changes promote L cell differentiation and metabolic improvements. Proinflammatory cytokines, such as interferon γ (IFNγ) and tumor necrosis factor alpha (TNF-α) can act on intestinal stem/progenitors to drive alterations in EEC development. We then took advantage of organoid cultures and *Vil-Cre*$^{+}$*;R26-rOGT* mice to modulate OGT levels without affecting the inflammatory gene program and were able to demonstrate that OGT directly inhibits L cell development. Taken together, these data indicate that defective protein O-GlcNAcylation can be a unifying pathogenic mechanism for microbial dysbiosis, intestinal inflammation, and EEC hyperplasia in IBD.

The *Ngn3*$^{+}$ lineage in the intestine is essential for life because loss of EECs in mice impairs lipid absorption, alters glucose metabolism, and leads to frequent perinatal death (Mellitzer et al., 2010). On the other hand, L cell hyperplasia, hormone hyper-secretion, and receptor agonism reduce food intake and ameliorate diabetes. Consistently, improved glucose metabolism and decreased body weight were observed in *Vil-Ogt* KO mice, in which EEC development was boosted. However, we only found very mild metabolic phenotypes in *Vil-Cre*$^{+}$*;R26-rOGT* mice, in which L cell numbers were reduced. No significant changes in body weight, glucose tolerance, insulin tolerance, or gastrointestinal motility were observed in mice fed with normal chow or an HFD (Figure 5; data not shown). This disparity could be due to the fact that L cells and GLP-1 levels were the primary targets of OGT overexpression in *Vil-Cre*$^{+}$*;R26-rOGT* mice, whereas most EEC types were affected in *Vil-Ogt* KO mice. In fact, when gut-derived GLP-1 was genetically deleted in mice, relatively mild impairments of glucose tolerance and gastric emptying were noticed (Chambers et al., 2017; Song et al., 2019). Therefore, we do not think that the L cell hyperplasia observed in *Vil-Ogt* KO mice is enough to drive the substantial improvement in body weight and glucose metabolism. Microbial dysbiosis caused by *Vil-Ogt* KO could reduce the gain of body weight and fat when transplanted into GF mice. Thus, we speculate that GLP-1 hypersecretion and perturbed gut microbiota together result in the metabolic changes observed in *Vil-Ogt* KO mice. It is also possible that intestinal epithelial damage and inflammation caused by OGT deletion contribute to the evident weight loss in *Vil-Ogt* KO mice.

In summary, we show that O-GlcNAc signaling in intestinal epithelial cells, controlled by the gut microbiota and nutrient availability, suppresses *Ngn3* transcription via FOXO1 O-GlcNAcylation, restrains EEC development, and modulates whole-body energy and glucose metabolism. Therefore, harnessing the hexosamine synthetic pathway and protein O-GlcNAcylation can be a future strategy for treatment of obesity and diabetes.

STAR★METHODS

RESOURCE AVAILABILITY

Lead Contact—Requests for further information and resources can be directed to the Lead Contact, Hai-Bin Ruan (hruan@umn.edu).

Materials Availability—Unique reagents generated in this study are available with a completed Material Transfer Agreement.

Data and Code Availability—The accession number for the 16S-seq data reported in this paper is Sequence Read Archive (SRA) repository: PRJNA644017.

EXPERIMENTAL MODEL AND SUBJECT DETAILS

Animals—*Ogt-floxed* mice (Shafi et al., 2000) and *Rosa26-rOGT-floxed* on the C57BL/6 background were kindly provided by Dr. Xiaoyong Yang (Yang et al., 2020). *Villin-Cre* mice (stock no. 004586) and *Neurog3-Cre* mice (stock no. 006333) were purchased from the Jackson Laboratory. Germ free mice on the C57BL/6 background were purchased from Taconic Biosciences together with age and sex matched C57BL/6 SPF mice as control. 5 pairs of them were euthanized immediately upon arrival for tissue collection. 10 extra germ free mice were used in fecal microbiota colonization experiments. Homozygous floxed $Ogt^{F/F}$ mice were bred to *Villin-Cre* and *Neurog3-Cre* mice to generate *Vil-Ogt* KO and *Ngn3-Ogt* KO mice, respectively. Homozygous floxed *Rosa26-rOGT* $^{F/F}$ mice were bred to *Villin-Cre* mice to generate *Vil-rOGT Tg* mice. 3-week to 4-month old mice were used for experiments. Age of mice in each experiment was specified in figure legends. All animals were kept on a 14 h: 10 h light: dark cycle in the animal facility at the University of Minnesota. Mice were group-housed unless otherwise mentioned, with free to access water and standard chow diet. All procedures involving animals were conducted within IACUC guidelines under approved protocols.

Ileal organoid and Caco-2 cell culture—Isolated ileal crypts were counted and cultured in Matrigel following a published protocol (Mahe et al., 2013). Growth medium consists of Advanced DMEM/F12 with Glutamax, HEPES, Pen/Strep, 1x N2 supplement, 1x B27 supplement, EGF (50 ng/ml), Noggin (100 ng/ml), and R-spondin conditioned media. Organoids were maintained at 37°C and medium was changed every 3 days. Cultures were split weekly by mechanical disruption of organoids. Passage 3-5 were used for experiments. Organoids were treated with 50 μM OSMI-1, SCFAs (5 mM acetate, 1 mM butyrate and propionate) (Pearce et al., 2020) and/or AS1842856 (Calbiochem, 1 μM) (Galley et al., 2019) for 2 days. Then medium was collected for GLP-1 measurement and organoids were subjected to RNA extraction or GLP-1 staining. Caco-2 cells were cultured as described previously (Natoli et al., 2012). Differentiated Caco-2 cells were serum starved overnight and treated with SCFAs (8 μM each) for 24 h before being subjected to protein extraction.

METHOD DETAILS

Metabolic assays—Body weights were monitored every week. Body composition was assessed using an EchoMRI system (Wang et al., 2018). For food intake measurement, mice were individually housed and food consumption was weighed every morning for 7 consecutive days. For the metabolic cage study, mice were first acclimated in metabolic chambers (Columbus Instruments), and then physical activity and energy expenditure were measured continuously for at least 2 days (Huang et al., 2014). For oral glucose-, and insulin-tolerance tests. 16 h fasted mice were given glucose (1.5 g/kg body weight) by gavage; 6 h fasted mice were injected with insulin (1 U/kg body weight) intraperitoneally. Tail-vein blood collected at the designated times was used to measure blood glucose level using a Contour Glucometer (Bayer). HOMA-IR was calculated as fasting insulin level x fasting glucose level. Serum insulin (EZRMI-13K) and active GLP-1 (EGLP-35K) were determined using ELISA kit (Millipore) following manufacture's instruction. To measure GI transit time, mice were fasted overnight and given a semiliquid methyl cellulose solution containing 0.1% Trypan blue by gavage. The time for expulsion of the fist blue feces pellet was determined as gastrointestinal transit time.

Fecal microbiota colonization—Donor mice were euthanized and ceca were aseptically removed immediately. The content was diluted 1:10 in a 50% glycerol/PBS solution and frozen at −80°C. On the day of inoculation, the cecal content was further diluted 1:5 in autoclaved PBS prior to oral gavage of 0.15 mL per mouse. Prior to inoculation, recipient animals were treated with a cocktail of broad-spectrum antibiotics to deplete gut microbiota (Hill et al., 2010; Reikvam et al., 2011). Specifically, animals having free access to autoclaved food and water were subjected to oral gavage daily for 14 days with 100 ul of autoclaved water supplemented with ampicillin (2 mg/ml), gentamicin (2 mg/ml), metronidazole (2 mg/ml), neomycin (2 mg/ml), and vancomycin (1 mg/ml). The germ-free recipient mice were inoculated immediately upon arrival at the University of Minnesota animal facility, and housed in SPF environment thereafter. A second inoculation was given 2 weeks later. Metabolic assays were carried out at indicated time points after transplantation.

Short chain fatty acids (SCFAs) treatment—Mice were treated with a cocktail of broad-spectrum antibiotics to deplete gut microbiota as mentioned above. Then sodium butyrate alone (3g/kg BW) or a mixture of sodium acetate, sodium propionate and sodium butyrate (1g of each SCFA/kg BW) were dissolved into saline and given by gavage 24h and 4 h before sacrifice.

***In vivo* intestinal barrier function assays—**Mice were fasted for 2-h and orally gavaged with fluorescein isothiocyanate (FITC)-dextran (average molecular weight: 3,000–5,000, 0.6 mg/g; Sigma) diluted in PBS. Fluorescence intensity of plasma samples was measured (excitation 492 nm/emission 520 nm) 4 h after the gavage.

16S rRNA gene sequencing—Total DNA in stool and cecal contents was extracted using the PowerFecal DNA Isolation Kit (Mo Bio). The V4 region of the bacterial 16S rRNA gene was amplified by triplicate PCR (F515/R806) using barcoded fusion primers. Samples were pooled in sets with a maximum of 96 samples in equal quantities. Paired-end

sequencing of the amplicon library was performed on the Illumina MiSeq 300-bp paired-end platform at the University of Minnesota Genomics Center (Gohl et al., 2016). A multistep bioinformatics analysis was performed using the QIIME 1.9.1 software, including filtering raw fastq files for primer and adaptor dimer sequences, removing contaminating host sequences and chimeric sequences, clustering sequences into operational taxonomic units (OTUs) using the open reference OTU calling method with the green genes 16S reference, and calculating alpha and beta diversity metrics. Linear discriminant analysis (LDA) effect size (LEfSe) method was used for microbial biomarker discovery (Segata et al., 2011).

Chemicals, plasmids, transfection, and luciferase assay—OSMI-1 (Sigma, 50 μM), 6-Ac-CAS (GlycoSyn, 10 μM), PUGNAc (Toronto Research Chemicals, 10 μM) were used when indicated. The Myc-hOGT plasmid was provided by Dr. Xiaochun Yu at the University of Michigan (Chen et al., 2013). *Ngn3-luc* was generated by inserting a ~4.1 kb promoter of the mouse *Ngn3* gene into the pGL3-basic vector. *IRE-luc* was generated by inserting the −1985 to −280 bp upstream of the mouse *Irs2* gene that contains two insulin-response elements (IREs) into the pGL3-basic vector. pCMV6-mNgn3-Myc-DDK (#MR212139) was purchased from Origene. pCMV-FOXO1 (#12148) was purchased from Addgene. pCMV-FOXO-4A was generated with the QuikChange XL II Site-Directed Mutagenesis Kit (Agilent). HepG2 and Caco-2 cells were transfected with expression plasmids, luciferase reporters, and β-galactosidase or Renilla-luciferase using Lipofectamine 3000 (Invitrogen) or FuGENE HD (Promega). Cells were lysed and luciferase and β-galactosidase enzyme activities were measured using kits from Promega. Relative luciferase activity was determined by normalizing to β-galactosidase or Renilla-luc activity (Ruan et al., 2012; Wang et al., 2018).

Histology, immunohistochemistry, and immunofluorescence—Tissues and organoids were fixed in 10% neutral buffered formalin. Organoids were then embedded in 5% gelatin before paraffin embedding. Immunohistochemistry was carried out using Histostain-Plus 3rd Gen IHC Detection Kit (Life technologies) following manufacturer's instruction. Antigen retrieval was performed in Citric buffer using a 2100 Retriever (Aptum Biologics). For immunofluorescence, tissue slides were blocked with 3% BSA, 0.2% TWEEN 20 in PBS, incubated with primary antibodies (1:100 to 1:200 dilution) overnight, and secondary antibodies (Alexa Fluor 488 anti-Rabbit IgG and anti-Mouse IgG, 1:400) for 1h. A Nikon system was used for fluorescence detection. For cell number quantification, 3-5 random fields per sample were captured. Stained cell specifically on the epithelium were counted. In the intestine, cell number was normalized to the number of crypt/villus units (ileum) or crypts (colon). In the organoid, cell number was normalized to nuclei number as indicated by DAPI staining. For the quantification of O-GlcNAcylation intensity in intestinal epithelium, the nucleus and cytoplasm region in the epithelium were selected and quantification was performed by FIJI.

Immunoprecipitation and Western Blot—Tissues were lysed in RIPA buffer containing proteinase inhibitors, protein phosphatase inhibitors and an OGA inhibitor. For immunoprecipitation, whole-cell lysates were incubated with and precipitated by anti-Flag beads (Millipore Sigma). Equal amounts of whole lysates or immunoprecipitation samples

were electrophoresed on TGX precast gels (Bio-Rad) and transferred to nitrocellulose membrane. Membranes were incubated with primary antibodies at 4°C for overnight. Western blotting was visualized by using IRDye secondary antibodies and the Odyssey imaging system (LI-COR Biosciences).

RNA and real time PCR—Total RNA was extracted from mouse tissues and organoids using TRIzol reagent (Invitrogen). cDNA was reverse transcribed (BioRad) and amplified with SYBR Green Supermix (Bio-Rad) using a C1000 Thermal Cycler (Bio-Rad). All data were normalized to the expression of the *Rplp0* gene. Primer sequences are listed in Table S2.

QUANTIFICATION AND STATISTICAL ANALYSIS

N values ≥ 3 and ≥ 4 were used for *in vitro* and *in vivo* experiments, respectively. The statistical comparisons were carried out using two-tailed unpaired Student's t test and one-way or two-way ANOVA with indicated post hoc tests with Prism 7 (Graphpad). Differences were considered significant when $p < 0.05$. Results are shown as mean ± SEM. *, $p < 0.05$; **, $p < 0.01$; ***, $p < 0.001$.

Supplementary Material

Refer to Web version on PubMed Central for supplementary material.

ACKNOWLEDGMENTS

We thank Drs. Alessandro Bartolomucci, Maria Razzoli, and Pilar Ariza Guzman for help with the metabolic cages and EchoMRI analyses. This work was supported by the National Natural and Science Foundation of China, China (81770543 to H.-B.R. and U1904132 to X.X.), American Diabetes Association, United States (1-18-IBS-167 to H.-B.R.), and the NIH, United States (R01 AI139420 and R21 AI140109 to H.-B.R., R21 DK112144 and R01 DK115720 to E.U.A., and R01 DK089098 and R01 DK102648 to X.Y.).

REFERENCES

Al-Masri M, Krishnamurthy M, Li J, Fellows GF, Dong HH, Goodyer CG, and Wang R (2010). Effect of forkhead box O1 (FOXO1) on beta cell development in the human fetal pancreas. Diabetologia 53, 699–711. [PubMed: 20033803]

Alejandro EU, Bozadjieva N, Kumusoglu D, Abdulhamid S, Levine H, Haataja L, Vadrevu S, Satin LS, Arvan P, and Bernal-Mizrachi E (2015). Disruption of O-linked N-Acetylglucosamine Signaling Induces ER Stress and β Cell Failure. Cell Rep. 13, 2527–2538. [PubMed: 26673325]

Arora T, Akrami R, Pais R, Bergqvist L, Johansson BR, Schwartz TW, Reimann F, Gribble FM, and Bäckhed F (2018). Microbial regulation of the L cell transcriptome. Sci. Rep 8, 1207. [PubMed: 29352262]

Barker N, van Es JH, Kuipers J, Kujala P, van den Born M, Cozijnsen M, Haegebarth A, Korving J, Begthel H, Peters PJ, and Clevers H (2007). Identification of stem cells in small intestine and colon by marker gene Lgr5. Nature 449, 1003–1007. [PubMed: 17934449]

Bond MR, and Hanover JA (2013). O-GlcNAc cycling: a link between metabolism and chronic disease. Annu. Rev. Nutr 33, 205–229. [PubMed: 23642195]

Bouchi R, Foo KS, Hua H, Tsuchiya K, Ohmura Y, Sandoval PR, Ratner LE, Egli D, Leibel RL, and Accili D (2014). FOXO1 inhibition yields functional insulin-producing cells in human gut organoid cultures. Nat. Commun 5, 4242. [PubMed: 24979718]

Brandt SJ, Götz A, Tschöp MH, and M€ller TD. (2018). Gut hormone polyagonists for the treatment of type 2 diabetes. Peptides 100, 190–201. [PubMed: 29412819]

Cantini G, Mannucci E, and Luconi M (2016). Perspectives in GLP-1 Research: New Targets, New Receptors. Trends Endocrinol. Metab 27, 427–438. [PubMed: 27091492]

Chambers AP, Sorrell JE, Haller A, Roelofs K, Hutch CR, Kim KS, Gutierrez-Aguilar R, Li B, Drucker DJ, D'Alessio DA, et al. (2017). The Role of Pancreatic Preproglucagon in Glucose Homeostasis in Mice. Cell Metab. 25, 927–934.e3. [PubMed: 28325479]

Chen Q, Chen Y, Bian C, Fujiki R, and Yu X (2013). TET2 promotes histone O-GlcNAcylation during gene transcription. Nature 493, 561–564. [PubMed: 23222540]

Cheng H, and Leblond CP (1974). Origin, differentiation and renewal of the four main epithelial cell types in the mouse small intestine. V. Unitarian Theory of the origin of the four epithelial cell types. Am. J. Anat 141, 537–561. [PubMed: 4440635]

den Besten G, van Eunen K, Groen AK, Venema K, Reijngoud DJ, and Bakker BM (2013). The role of short-chain fatty acids in the interplay between diet, gut microbiota, and host energy metabolism. J. Lipid Res 54,2325–2340. [PubMed: 23821742]

Drucker DJ (2016). The Cardiovascular Biology of Glucagon-like Peptide-1. Cell Metab. 24, 15–30. [PubMed: 27345422]

Egerod KL, Engelstoft MS, Grunddal KV, Nøhr MK, Secher A, Sakata I , Pedersen J, Windelov JA, FGchtbauer EM, Olsen J, et al. (2012). A major lineage of enteroendocrine cells coexpress CCK, secretin, GIP, GLP-1, PYY, and neurotensin but not somatostatin. Endocrinology 153, 5782–5795. [PubMed: 23064014]

Faerch K, Torekov SS, Vistisen D, Johansen NB, Witte DR, Jonsson A, Pedersen O, Hansen T, Lauritzen T, Sandbaek A, et al. (2015). GLP-1 Response to Oral Glucose Is Reduced in Prediabetes, Screen-Detected Type 2 Diabetes, and Obesity and Influenced by Sex: The ADDITION-PRO Study. Diabetes 64, 2513–2525. [PubMed: 25677912]

Fardini Y, Masson E, Boudah O, Ben Jouira R, Cosson C, Pierre-Eugene C, Kuo MS, and Issad T (2014). O-GlcNAcylation of FoxO1 in pancreatic β cells promotes Akt inhibition through an IGFBP1-mediated autocrine mechanism. FASEB J. 28, 1010–1021. [PubMed: 24174424]

Galley JC, Durgin BG, Miller MP, Hahn SA, Yuan S, Wood KC, and Straub AC (2019). Antagonism of Forkhead Box Subclass O Transcription Factors Elicits Loss of Soluble Guanylyl Cyclase Expression. Mol. Pharmacol 95, 629–637. [PubMed: 30988014]

Gehart H, van Es JH, Hamer K, Beumer J, Kretzschmar K, Dekkers JF, Rios A, and Clevers H (2019). Identification of Enteroendocrine Regulators by Real-Time Single-Cell Differentiation Mapping. Cell 176, 1158–1173.e16. [PubMed: 30712869]

Gil-Lozano M, Wu WK, Martchenko A, and Brubaker PL (2016). High-Fat Diet and Palmitate Alter the Rhythmic Secretion of Glucagon-Like Peptide-1 by the Rodent L-cell. Endocrinology 157, 586–599. [PubMed: 26646204]

Gohl DM, Vangay P, Garbe J, MacLean A, Hauge A, Becker A, Gould TJ, Clayton JB, Johnson TJ, Hunter R, et al. (2016). Systematic improvement of amplicon marker gene methods for increased accuracy in microbiome studies. Nat. Biotechnol. 34, 942–949. [PubMed: 27454739]

Gribble FM, and Reimann F (2016). Enteroendocrine Cells: Chemosensors in the Intestinal Epithelium. Annu. Rev. Physiol 78, 277–299. [PubMed: 26442437]

Haber AL, Biton M, Rogel N, Herbst RH, Shekhar K, Smillie C, Burgin G , Delorey TM, Howitt MR, Katz Y, et al. (2017).A single-cell survey of the small intestinal epithelium. Nature 551, 333–339. [PubMed: 29144463]

Habib AM, Richards P, Cairns LS, Rogers GJ, Bannon CA, Parker HE, Morley TC, Yeo GS, Reimann F, and Gribble FM (2012). Overlap of endocrine hormone expression in the mouse intestine revealed by transcriptional profiling and flow cytometry. Endocrinology 153, 3054–3065. [PubMed: 22685263]

Hanover JA, Krause MW, and Love DC (2012). Bittersweet memories: linking metabolism to epigenetics through O-GlcNAcylation. Nat. Rev. Mol. Cell Biol 13,312–321. [PubMed: 22522719]

Hart GW, Housley MP, and Slawson C (2007). Cycling of O-linked beta-N-acetylglucosamine on nucleocytoplasmic proteins. Nature 446, 1017–1022. [PubMed: 17460662]

Hart GW, Slawson C, Ramirez-Correa G, and Lagerlof O (2011). Cross talk between O-GlcNAcylation and phosphorylation: roles in signaling, transcription, and chronic disease. Annu. Rev. Biochem 80, 825–858. [PubMed: 21391816]

Hill DA, Hoffmann C, Abt MC, Du Y, Kobuley D, Kirn TJ, Bushman FD, and Artis D (2010). Metagenomic analyses reveal antibiotic-induced temporal and spatial changes in intestinal microbiota with associated alterations in immune cell homeostasis. Mucosal Immunol. 3, 148–158. [PubMed: 19940845]

Holst JJ (2013). Enteroendocrine secretion of gut hormones in diabetes, obesity and after bariatric surgery. Curr. Opin. Pharmacol 13, 983–988. [PubMed: 24161809]

Housley MP, Rodgers JT, Udeshi ND, Kelly TJ, Shabanowitz J, Hunt DF, Puigserver P, and Hart GW (2008). O-GlcNAc regulates FoxO activation in response to glucose. J. Biol. Chem 283, 16283–16292. [PubMed: 18420577]

Huang Z, Ruan HB, Xian L, Chen W, Jiang S, Song A, Wang Q, Shi P, Gu X, and Gao X (2014). The stem cell factor/Kit signalling pathway regulates mitochondrial function and energy expenditure. Nat. Commun 5,4282. [PubMed: 24999927]

Hutch CR, and Sandoval D (2017). The Role of GLP-1 in the Metabolic Success of Bariatric Surgery. Endocrinology 158, 4139–4151. [PubMed: 29040429]

Jenny M, Uhl C, Roche C, Duluc I, Guillermin V, Guillemot F, Jensen J, Kedinger M, and Gradwohl G (2002). Neurogenin3 is differentially required for endocrine cell fate specification in the intestinal and gastric epithelium. EMBO J. 21,6338–6347. [PubMed: 12456641]

Joiner CM, Li H, Jiang J, and Walker S (2019). Structural characterization of the O-GlcNAc cycling enzymes: insights into substrate recognition and catalytic mechanisms. Curr. Opin. Struct. Biol 56, 97–106. [PubMed: 30708324]

Kasubuchi M, Hasegawa S, Hiramatsu T, Ichimura A, and Kimura I (2015). Dietary gut microbial metabolites, short-chain fatty acids, and host metabolic regulation. Nutrients 7, 2839–2849. [PubMed: 25875123]

Knip M, and Siljander H (2016). The role of the intestinal microbiota in type 1 diabetes mellitus. Nat. Rev. Endocrinol 12, 154–167. [PubMed: 26729037]

Larraufie P, Martin-Gallausiaux C, Lapaque N, Dore J, Gribble FM, Reimann F, and Blottiere HM (2018). SCFAs strongly stimulate PYY production in human enteroendocrine cells. Sci. Rep 8, 74. [PubMed: 29311617]

Larsson LI, St-Onge L, Hougaard DM, Sosa-Pineda B, and Gruss P (1998). Pax 4 and 6 regulate gastrointestinal endocrine cell development. Mech. Dev 79, 153–159. [PubMed: 10349628]

Latorre R, Sternini C, De Giorgio R, and Greenwood-Van Meerveld B (2016). Enteroendocrine cells: a review of their role in brain-gut communication. Neurogastroenterol. Motil 28, 620–630. [PubMed: 26691223]

Lee CS, Perreault N, Brestelli JE, and Kaestner KH (2002). Neurogenin 3 is essential for the proper specification of gastric enteroendocrine cells and the maintenance of gastric epithelial cell identity. Genes Dev. 16, 1488–1497. [PubMed: 12080087]

Liu B, Salgado OC, Singh S, Hippen KL, Maynard JC, Burlingame AL, Ball LE, Blazar BR, Farrar MA, Hogquist KA, and Ruan HB (2019). The lineage stability and suppressive program of regulatory T cells require protein O-GlcNAcylation. Nat. Commun 10, 354. [PubMed: 30664665]

Mahe MM, Aihara E, Schumacher MA, Zavros Y, Montrose MH, Helmrath MA, Sato T, and Shroyer NF (2013). Establishment of Gastrointestinal Epithelial Organoids. Curr. Protoc. Mouse Biol 3, 217–240. [PubMed: 25105065]

Mellitzer G, Beucher A, Lobstein V, Michel P, Robine S, Kedinger M, and Gradwohl G (2010). Loss of enteroendocrine cells in mice alters lipid absorption and glucose homeostasis and impairs postnatal survival. J. Clin. Invest 120, 1708–1721. [PubMed: 20364088]

Moran-Ramos S, Tovar AR, and Torres N (2012). Diet: friend or foe of enteroendocrine cells-how it interacts with enteroendocrine cells. Adv. Nutr 3, 8–20. [PubMed: 22332097]

Mutoh H, Fung BP, Naya FJ, Tsai MJ, Nishitani J, and Leiter AB (1997). The basic helix-loop-helix transcription factor BETA2/NeuroD is expressed in mammalian enteroendocrine cells and activates secretin gene expression. Proc. Natl. Acad. Sci. USA 94, 3560–3564. [PubMed: 9108015]

Natoli M, Leoni BD, D'Agnano I, Zucco F, and Felsani A (2012). Good Caco-2 cell culture practices. Toxicol. In Vitro 26, 1243–1246. [PubMed: 22465559]

Naya FJ, Huang HP, Qiu Y, Mutoh H, DeMayo FJ, Leiter AB, and Tsai MJ (1997). Diabetes, defective pancreatic morphogenesis, and abnormal enteroendocrine differentiation in BETA2/neuroD-deficient mice. Genes Dev. 11, 2323–2334. [PubMed: 9308961]

Nøhr MK, Pedersen MH, Gille A, Egerod KL, Engelstoft MS, Husted AS, Sichlau RM, Grunddal KV, Poulsen SS, Han S, et al. (2013). GPR41/FFAR3 and GPR43/FFAR2 as cosensors for short-chain fatty acids in enteroendocrine cells vs FFAR3 in enteric neurons and FFAR2 in enteric leukocytes. Endocrinology 154, 3552–3564. [PubMed: 23885020]

Nøhr MK, Egerod KL, Christiansen SH, Gille A, Offermanns S, Schwartz TW, and Moller M (2015). Expression of the short chain fatty acid receptor GPR41/FFAR3 in autonomic and somatic sensory ganglia. Neuroscience 290, 126–137. [PubMed: 25637492]

Ortiz-Meoz RF, Jiang J, Lazarus MB, Orman M, Janetzko J, Fan C, Duveau DY, Tan ZW, Thomas CJ, and Walker S (2015). A small molecule that inhibits OGT activity in cells. ACS Chem. Biol 10, 1392–1397. [PubMed: 25751766]

Pearce SC, Weber GJ, van Sambeek DM, Soares JW, Racicot K, and Breault DT (2020). Intestinal enteroids recapitulate the effects of short-chain fatty acids on the intestinal epithelium. PLoS ONE 15, e0230231. [PubMed: 32240190]

Petersen N, Reimann F, Bartfeld S, Farin HF, Ringnalda FC, Vries RG, van den Brink S, Clevers H, Gribble FM, and de Koning EJ (2014). Generation of L cells in mouse and human small intestine organoids. Diabetes 63, 410–420. [PubMed: 24130334]

Psichas A, Sleeth ML, Murphy KG, Brooks L, Bewick GA, Hanyaloglu AC, Ghatei MA, Bloom SR, and Frost G (2015). The short chain fatty acid propionate stimulates GLP-1 and PYY secretion via free fatty acid receptor 2 in rodents. Int. J. Obes 39, 424–429.

Reikvam DH, Erofeev A, Sandvik A, Grcic V, Jahnsen FL, Gaustad P, McCoy KD, Macpherson AJ, Meza-Zepeda LA, and Johansen FE (2011). Depletion of murine intestinal microbiota: effects on gut mucosa and epithelial gene expression. PLoS ONE 6, e17996. [PubMed: 21445311]

Richards P, Pais R, Habib AM, Brighton CA, Yeo GS, Reimann F, and Gribble FM (2016). High fat diet impairs the function of glucagon-like peptide-1 producing L-cells. Peptides 77, 21–27. [PubMed: 26145551]

Rosenbaum M, Knight R, and Leibel RL (2015). The gut microbiota in human energy homeostasis and obesity. Trends Endocrinol. Metab 26, 493–501. [PubMed: 26257300]

Ruan HB, Han X, Li MD, Singh JP, Qian K, Azarhoush S, Zhao L, Bennett AM, Samuel VT, Wu J, et al. (2012). O-GlcNAc transferase/host cell factor C1 complex regulates gluconeogenesis by modulating PGC-1 a stability. Cell Metab. 16, 226–237. [PubMed: 22883232]

Ruan HB, Nie Y, and Yang X (2013a). Regulation of protein degradation by O-GlcNAcylation: crosstalk with ubiquitination. Mol. Cell. Proteomics 12, 3489–3497. [PubMed: 23824911]

Ruan HB, Singh JP, Li MD, Wu J, and Yang X (2013b). Cracking the O-GlcNAc code in metabolism. Trends Endocrinol. Metab 24, 301–309. [PubMed: 23647930]

Ruan HB, Dietrich MO, Liu ZW, Zimmer MR, Li MD, Singh JP, Zhang K, Yin R, Wu J, Horvath TL, and Yang X (2014). O-GlcNAc transferase enables AgRP neurons to suppress browning of white fat. Cell 159, 306–317. [PubMed: 25303527]

Ruan HB, Ma Y, Torres S, Zhang B, Feriod C, Heck RM, Qian K, Fu M, Li X, Nathanson MH, et al. (2017). Calcium-dependent O-GlcNAc signaling drives liver autophagy in adaptation to starvation. Genes Dev. 31, 1655–1665. [PubMed: 28903979]

Schonhoff SE, Giel-Moloney M, and Leiter AB (2004a). Minireview: Development and differentiation of gut endocrine cells. Endocrinology 145, 2639–2644. [PubMed: 15044355]

Schonhoff SE, Giel-Moloney M, and Leiter AB (2004b). Neurogenin 3-expressing progenitor cells in the gastrointestinal tract differentiate into both endocrine and non-endocrine cell types. Dev. Biol 270, 443–454. [PubMed: 15183725]

Segata N, Izard J, Waldron L, Gevers D, Miropolsky L, Garrett WS, and Huttenhower C (2011). Metagenomic biomarker discovery and explanation. Genome Biol. 12, R60. [PubMed: 21702898]

Shafi R, Iyer SP, Ellies LG, O'Donnell N, Marek KW, Chui D, Hart GW, and Marth JD (2000). The O-GlcNAc transferase gene resides on the X chromosome and is essential for embryonic stem cell viability and mouse ontogeny. Proc. Natl. Acad. Sci. USA 97, 5735–5739. [PubMed: 10801981]

Shroyer NF, Helmrath MA, Wang VY, Antalffy B, Henning SJ, and Zoghbi HY (2007). Intestine-specific ablation of mouse atonal homolog 1 (Math1) reveals a role in cellular homeostasis. Gastroenterology 132, 2478–2488. [PubMed: 17570220]

Song Y, Koehler JA, Baggio LL, Powers AC, Sandoval DA, and Drucker DJ (2019). Gut-Proglucagon-Derived Peptides Are Essential for Regulating Glucose Homeostasis in Mice. Cell Metab. 30, 976–986.e3. [PubMed: 31495689]

Tang C, Ahmed K, Gille A, Lu S, Grone HJ, Tunaru S, and Offermanns S (2015). Loss of FFA2 and FFA3 increases insulin secretion and improves glucose tolerance in type 2 diabetes. Nat. Med 21, 173–177. [PubMed: 25581519]

Toft-Nielsen MB, Damholt MB, Madsbad S, Hilsted LM, Hughes TE, Michelsen BK, and Holst JJ (2001). Determinants of the impaired secretion of glucagon-like peptide-1 in type 2 diabetic patients. J. Clin. Endocrinol. Metab 86, 3717–3723. [PubMed: 11502801]

Tolhurst G, Heffron H, Lam YS, Parker HE, Habib AM, Diakogiannaki E , Cameron J, Grosse J, Reimann F, and Gribble FM (2012). Short-chain fatty acids stimulate glucagon-like peptide-1 secretion via the G-protein-coupled receptor FFAR2. Diabetes 61, 364–371. [PubMed: 22190648]

Torres CR, and Hart GW (1984). Topography and polypeptide distribution of terminal N-acetylglucosamine residues on the surfaces of intact lymphocytes. Evidence for O-linked GlcNAc. J. Biol. Chem 259, 3308–3317. [PubMed: 6421821]

Tremaroli V, and Bäckhed F (2012). Functional interactions between the gut microbiota and host metabolism. Nature 489, 242–249. [PubMed: 22972297]

Troke RC, Tan TM, and Bloom SR (2014). The future role of gut hormones in the treatment of obesity. Ther. Adv. Chronic Dis 5, 4–14. [PubMed: 24381724]

Tschöp MH, Speakman JR, Arch JR, Auwerx J, Brining JC, Chan L, Eckel RH, Farese RV Jr., Galgani JE, Hambly C, et al. (2011). A guide to analysis of mouse energy metabolism. Nat. Methods 9, 57–63. [PubMed: 22205519]

Vilsbøll T, Krarup T, Deacon CF, Madsbad S, and Holst JJ (2001). Reduced postprandial concentrations of intact biologically active glucagonlike peptide 1 in type 2 diabetic patients. Diabetes 50, 609–613. [PubMed: 11246881]

Vocadlo DJ (2012). O-GlcNAc processing enzymes: catalytic mechanisms, substrate specificity, and enzyme regulation. Curr. Opin. Chem. Biol 16, 488–497. [PubMed: 23146438]

Wang Q, Tang J, Jiang S, Huang Z, Song A, Hou S, Gao X, and Ruan HB (2018). Inhibition of PPARγ, adipogenesis and insulin sensitivity by MAGED1. J. Endocrinol 239, 167–180. [PubMed: 30121577]

Wichmann A, Allahyar A, Greiner TU, Plovier H, Lundén GO, Larsson T , Drucker DJ, Delzenne NM, Cani PD, and Bäckhed F (2013). Microbial modulation of energy availability in the colon regulates intestinal transit. Cell Host Microbe 14, 582–590. [PubMed: 24237703]

Worthington JJ, Reimann F, and Gribble FM (2018). Enteroendocrine cells-sensory sentinels of the intestinal environment and orchestrators of mucosal immunity. Mucosal Immunol. 11, 3–20. [PubMed: 28853441]

Yang X, and Qian K (2017). Protein O-GlcNAcylation: emerging mechanisms and functions. Nat. Rev. Mol. Cell Biol 18, 452–465. [PubMed: 28488703]

Yang Q, Bermingham NA, Finegold MJ, and Zoghbi HY (2001). Requirement of Math1 for secretory cell lineage commitment in the mouse intestine. Science 294,2155–2158. [PubMed: 11739954]

Yang Y, Fu M, Li MD, Zhang K, Zhang B, Wang S, Liu Y, Ni W, Ong Q, Mi J, and Yang X (2020). O-GlcNAc transferase inhibits visceral fat lipolysis and promotes diet-induced obesity. Nat. Commun 11, 181. [PubMed: 31924761]

Zarrinpar A, Chaix A, Xu ZZ, Chang MW, Marotz CA, Saghatelian A, Knight R, and Panda S (2018). Antibiotic-induced microbiome depletion alters metabolic homeostasis by affecting gut signaling and colonic metabolism. Nat. Commun 9, 2872. [PubMed: 30030441]

Zhao M, Xiong X, Ren K, Xu B, Cheng M, Sahu C, Wu K, Nie Y, Huang Z, Blumberg RS, et al. (2018). Deficiency in intestinal epithelial O-GlcNAcylation predisposes to gut inflammation. EMBO Mol. Med 10, e8736. [PubMed: 29941542]

Zheng J, Xiao KL, Chen L, Wu C, Hu X, Zeng T, Chen XQ, Li WJ, Deng X, Li H, and Li YM (2017). Insulin sensitizers improve the GLP-1 secretion and the amount of intestinal L cells on high-fat-diet-induced catch-up growth. Nutrition 39-40, 82–91. [PubMed: 28606576]

Highlights

- O-GlcNAcylation in intestinal epithelial cells suppresses L cell differentiation
- FOXO1 O-GlcNAcylation inhibits *Ngn3* transcription
- SCFA-dependent O-GlcNAc is required for microbial regulation of L cell function
- Microbial dysbiosis in OGT-deficient mice contributes to improved metabolism

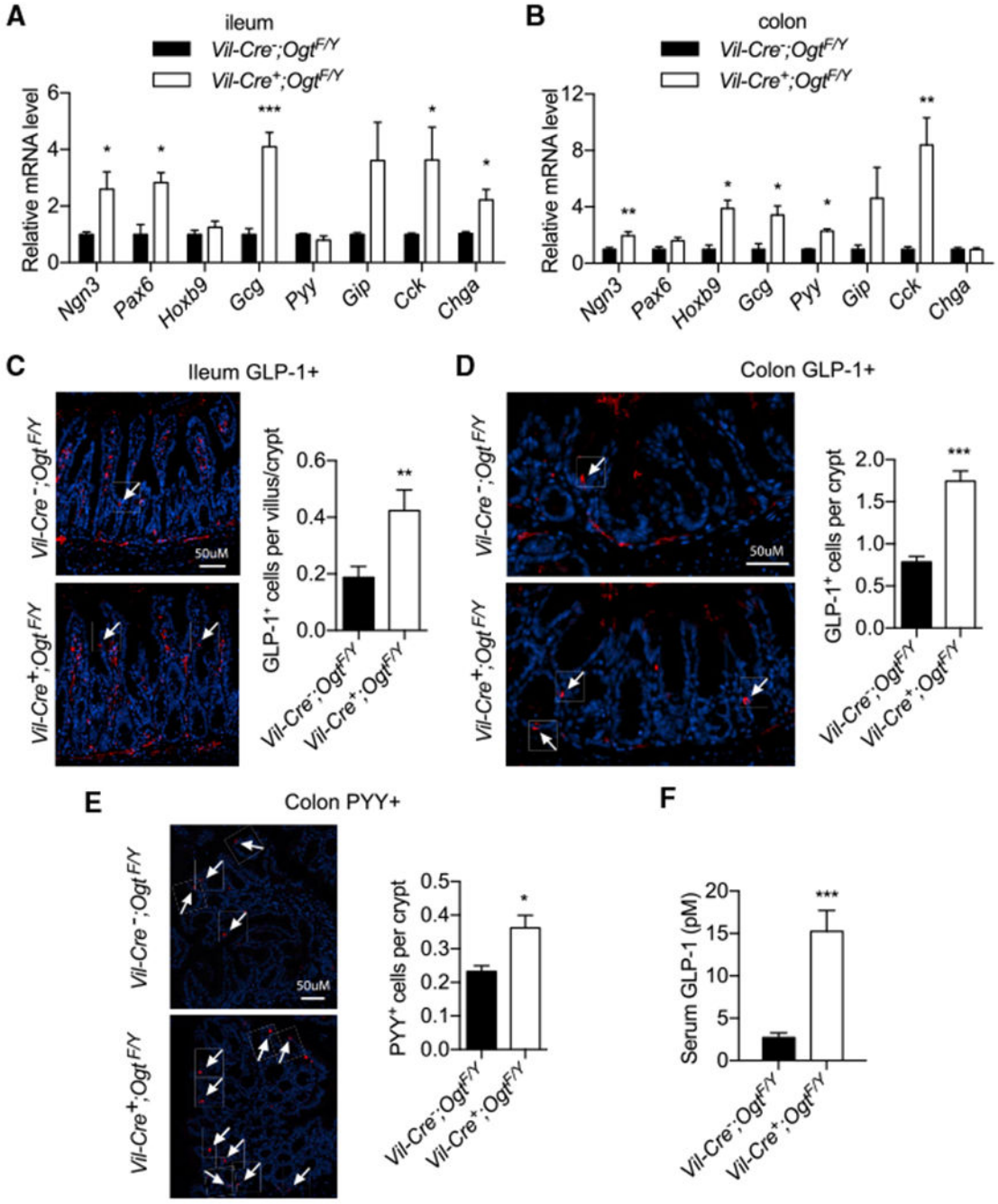

Figure 1. Loss of OGT in the Intestinal Epithelium Promotes EEC Development

(A and B) Expression of EEC marker genes in the ileum (A) and colon (B) of 2-month-old WT and *Vil-Ogt* KO male mice (n = 4–10).

(C–E) Representative images (left) and quantified numbers (right) of GLP-1$^+$ cells in the ileum (C, 133 and 92 crypt/villus units counted from 5 WT and 4 KO) and colon (D, 176 and 138 crypts counted from 5 WT and 5 KO) and PYY$^+$ cells in the colon (E, 1,005 and 867 crypts counted from 5 WT and 4 KO) of 10-week-old WT and *Vil-Ogt* KO male mice.

(F) Serum GLP-1 levels of WT (n = 9) and *Vil-Ogt* KO (n = 10) male mice at the age of 8–10 weeks.

Data are represented as mean ± SEM. *p < 0.05, **p < 0.01, ***p < 0.001 by two-tailed unpaired Student's t test.

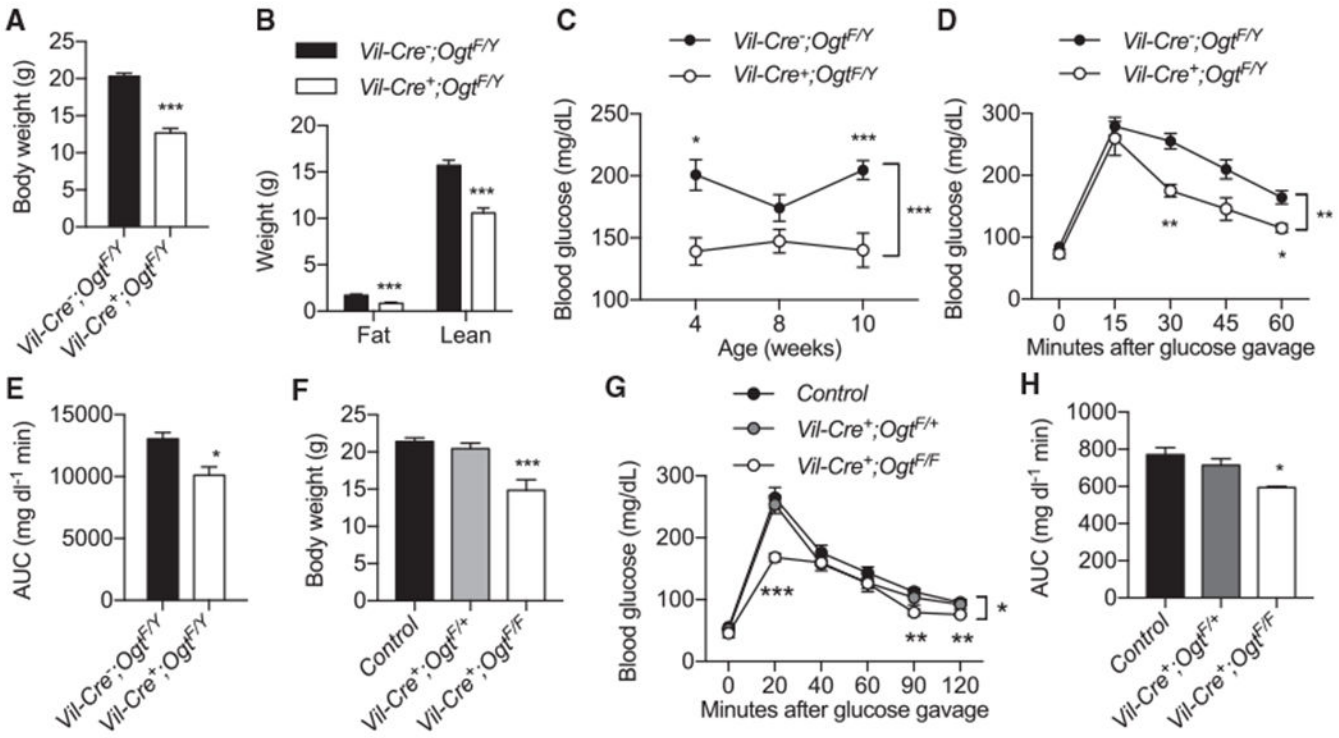

Figure 2. Improved Metabolism in *Vil-Ogt* KO Mice

(A and B) Body weight (A) and body composition (B) of 7-week-old control (n = 6) and *Vil-Ogt* KO (n = 5) male mice.

(C) Random blood glucose levels of control and *Vil-Ogt* KO male mice at the age of 4 (n = 2-5), 8 (n = 6), and 10 (n = 6) weeks.

(D and E) Oral glucose tolerance test of 7-week-old control (n = 6) and *Vil-Ogt* KO (n = 4) male mice (D). Area under the curve of (D) is shown in (E).

(F) Body weight of 9-week-old control (n = 11), heterozygous (n = 4), and homozygous (n = 5) *Vil-Ogt* KO female mice.

(G and H) Oral glucose tolerance test of 10- to 14-week-old control (n = 11), heterozygous (n = 3), and homozygous (n = 5) *Vil-Ogt* KO female mice (G). Area under the curve of (G) is shown in (H).

Data are represented as mean ± SEM. *p < 0.05, **p < 0.01, ***p < 0.001 by two-tailed unpaired Student's t test (A, B, and E), one-way ANOVA with post hoc Tukey's test (F and H), or two-way ANOVA with post hoc Sidak's test (C, D and G).

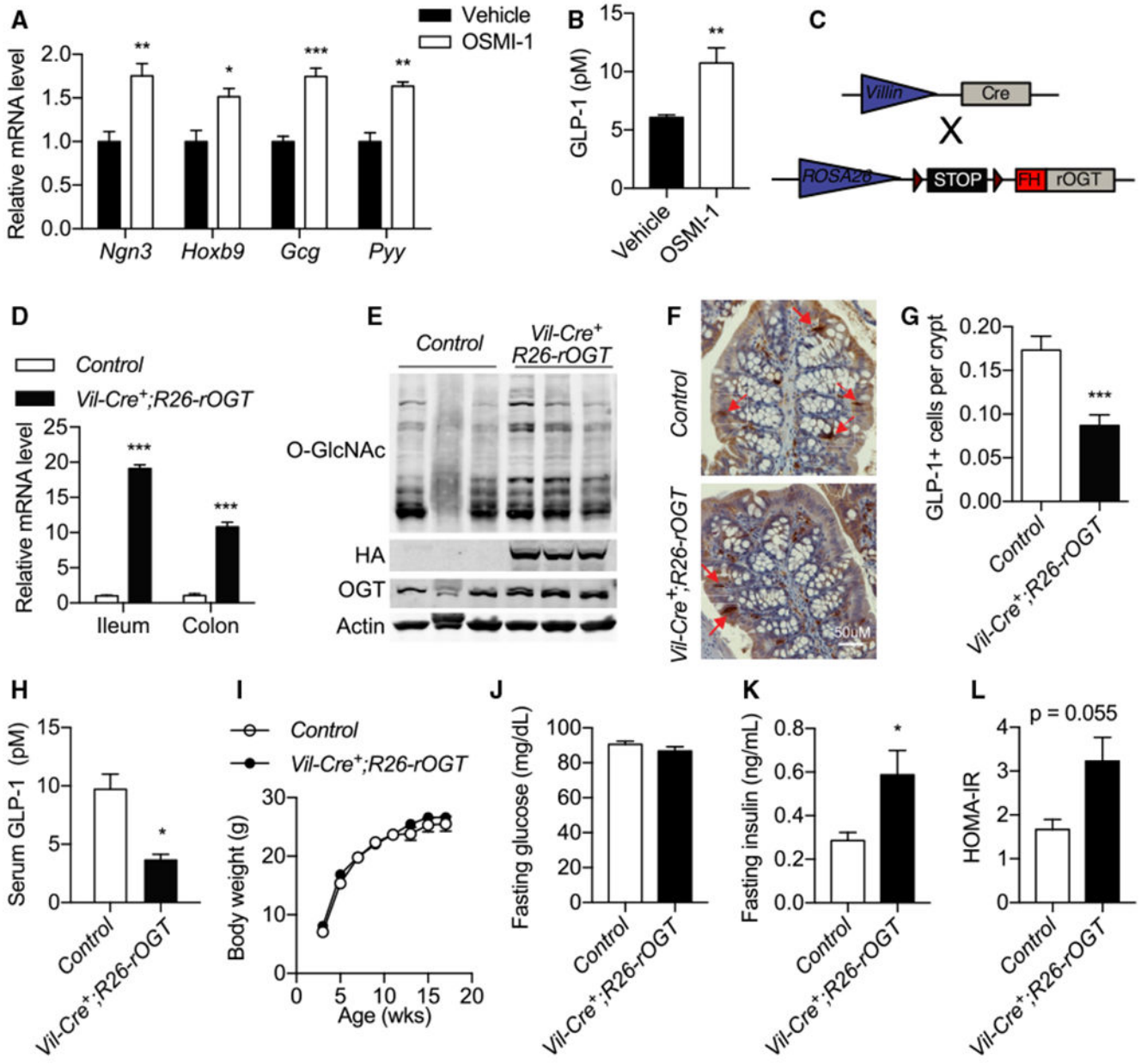

Figure 3. Protein O-GlcNAcylation Inhibits L Cell Development

(A and B) Ileal organoids were treated with vehicle or OSMI-1 for 2 days, and then gene expression (A) and GLP-1 secretion to the medium (B) were determined (n = 3).

(C) Schematic view of the *Rosa26-rOGT* locus and mating strategy to generate *Vil-Cre*$^{+}$*;R26-rOGT* mice.

(D) RNA levels of rat *Ogt* gene expression in the ileum and colon of 4-month-old control (n = 5) and *Vil-Cre*$^{+}$*;R26-rOGT* (n = 4) mice.

(E) Immunoblotting showing total protein O-GlcNAcylation, hemagglutinin (HA) tag, and OGT in the colon of control and *Vil-Cre*$^{+}$*;R26-rOGT* mice.

(F and G) Representative images (F) and quantified numbers of GLP-1$^+$ L cells (G) in the colon of 4-month-old control (756 crypts of 5 mice) and *Vil-Cre*$^+$*;R26-rOGT* (611 crypts of 4 animals) mice.

(H) Serum GLP-1 levels of control and *Vil-Cre*$^+$*;R26-rOGT* male mice (n = 3).

(I) Growth curve of control (n = 8) and *Vil-Cre*$^+$*;R26-rOGT* (n = 4) male mice fed normal chow.

(J–L) Levels of blood glucose (J), blood insulin (K), and calculated HOMA-IR (L) of overnight-fasted control (n = 8) and *Vil-Cre*$^+$*;R26-rOGT* (n = 4) male mice at the age of 4 months.

Data are represented as mean ± SEM. *p < 0.05, **p < 0.01, ***p < 0.001 by two-tailed unpaired Student's t test.

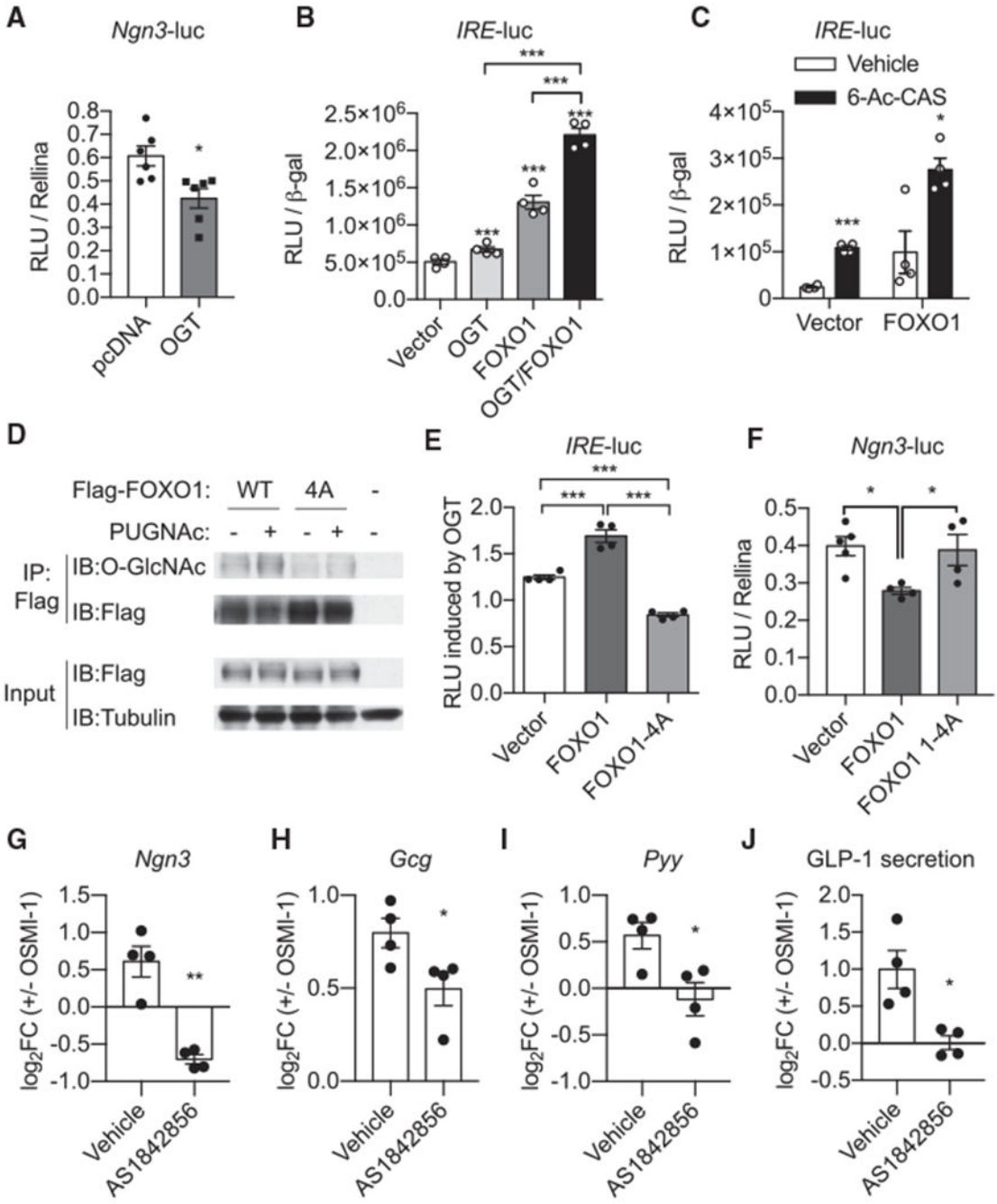

Figure 4. O-GlcNAcylation Modulates the Transcriptional Activity of FOXO1

(A) Transcriptional repressor of Ngn3-luciferase activity by OGT in Caco-2 cells (n = 6). RLU, relative luminescence unit.

(B and C) Transcriptional activation of FOXO1 on the insulin-responsive element (*IRE*) with OGT coexpression (B) or OGA inhibition (C). Luciferase activity was normalized to co-transfected β-galactosidase (β-gal) activity in HepG2 cells (n = 4).

(D) O-GlcNAcylation levels of WT- and 4A-FOXO1 expressed in 293 cells in the absence or presence of PUGNAc, an OGA inhibitor.

(E) Changes in the transcriptional activation activity of FOXO1 on the *IRE*-luciferase (luc) reporter after co-expression with OGT in HepG2 cells (n = 4).
(F) Transcriptional repression of Ngn3-luciferase activity by WT and 4A-FOXO1 in Caco-2 cells (n = 4–5).
(G–J) Ileal organoids were treated with or without OSMI-1 in the presence or absence of AS1842856 for 2 days (n = 4). Expression of the *Nng3* (G), *Gcg* (H), and *Pyy* (I) genes and GLP-1 secretion into the medium (J) were determined. Log2 values of fold change (FC) after OSMI-1 treatment were calculated and plotted.
Data are represented as mean ± SEM. *p < 0.05, **p < 0.01, ***p < 0.001 by two-tailed unpaired Student's t test (A and G–J), one-way ANOVA with post hoc Turkey's (B and E) or Dunnett's (F) test, or two-way ANOVA with post hoc Tukey's test (C).

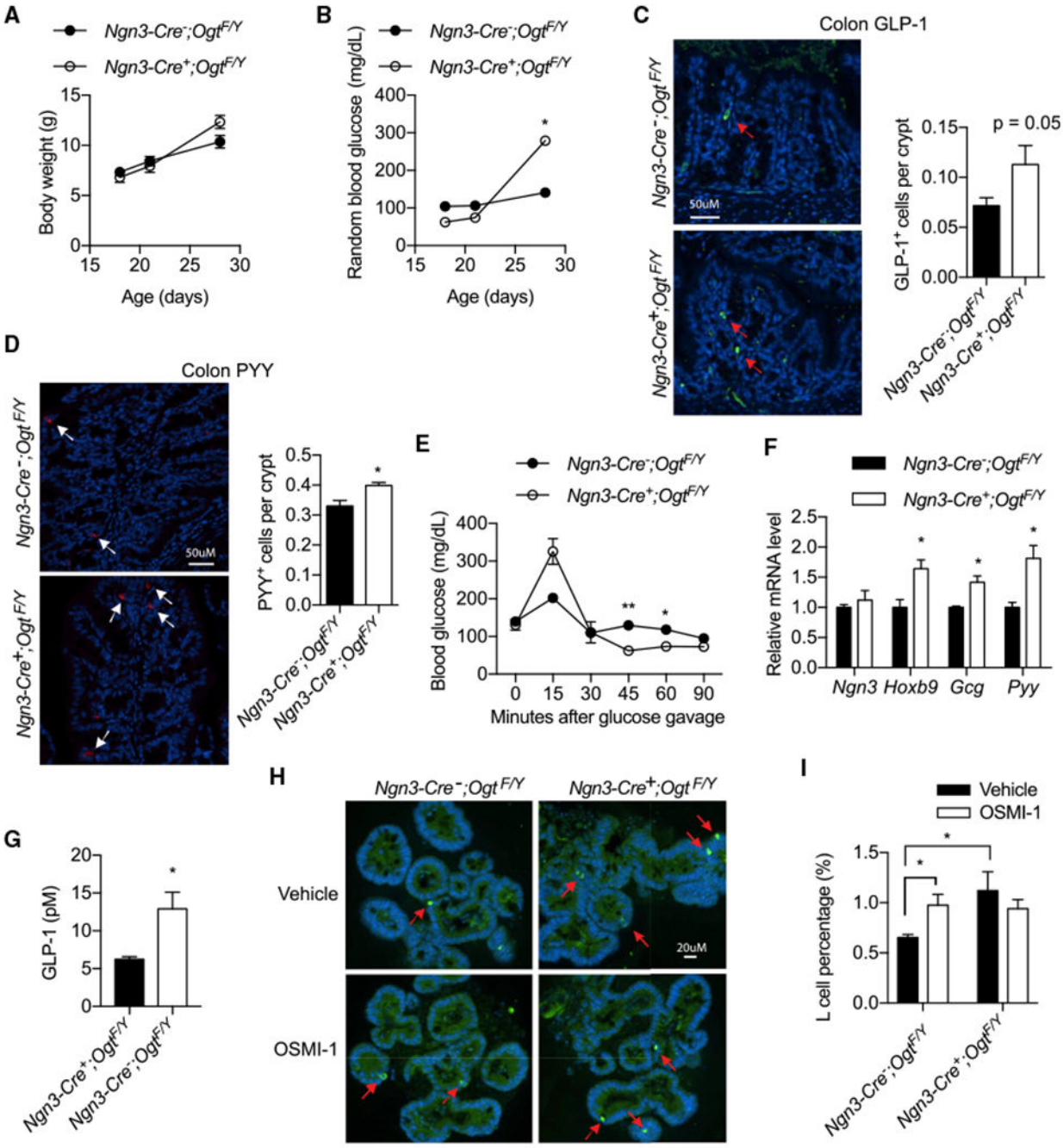

Figure 5. Loss of OGT in the *Ngn3* Lineage Promotes L cell Development

(A and B) Body weight (A) and random blood glucose (B) of WT and *Ngn3-Ogt* KO male mice at the indicated ages.

(C) Representative images (left) and quantified numbers (right) of GLP-1$^+$ L cells in the colon (187 and 235 crypts counted from 4 WT and 5 KO) of 3-week-old WT and *Ngn3-OGT* KO male mice.

(D) Representative images (left) and quantified numbers (right) of PYY^+ L cells in the colon (1,430 and 1,141 crypts counted from 4 WT and 5 KO) of 3-week-old WT and *Ngn3-Ogt* KO male mice.

(E) Oral glucose tolerance test of 3-week-old (n = 4–5) *Ngn3-Ogt* KO male mice and their littermate controls after 4 h of fasting.

(F) Ileal organoids from WT and *Ngn3-Ogt* KO male mice were cultured and collected to determine the expression of L cell marker genes by qRT-PCR (n = 4).

(G) Secretion of GLP-1 from WT and *Ngn3-Ogt* KO organoids into the medium, determined by ELISA (n = 6).

(H and I) Representative images (H) and quantified numbers (I) of $GLP\text{-}1^+$ L cells in WT and *Ngn3-Ogt* KO organoids treated with vehicle or OSMI-1 (n = 3–4). See also Table S1. Data are represented as mean ± SEM. *p < 0.05, **p < 0.01, ***p < 0.001 by two-tailed unpaired Student's t test (C, D, F, and G) or two-way ANOVA with post hoc Sidak's test (B and E) or Tukey's test (I).

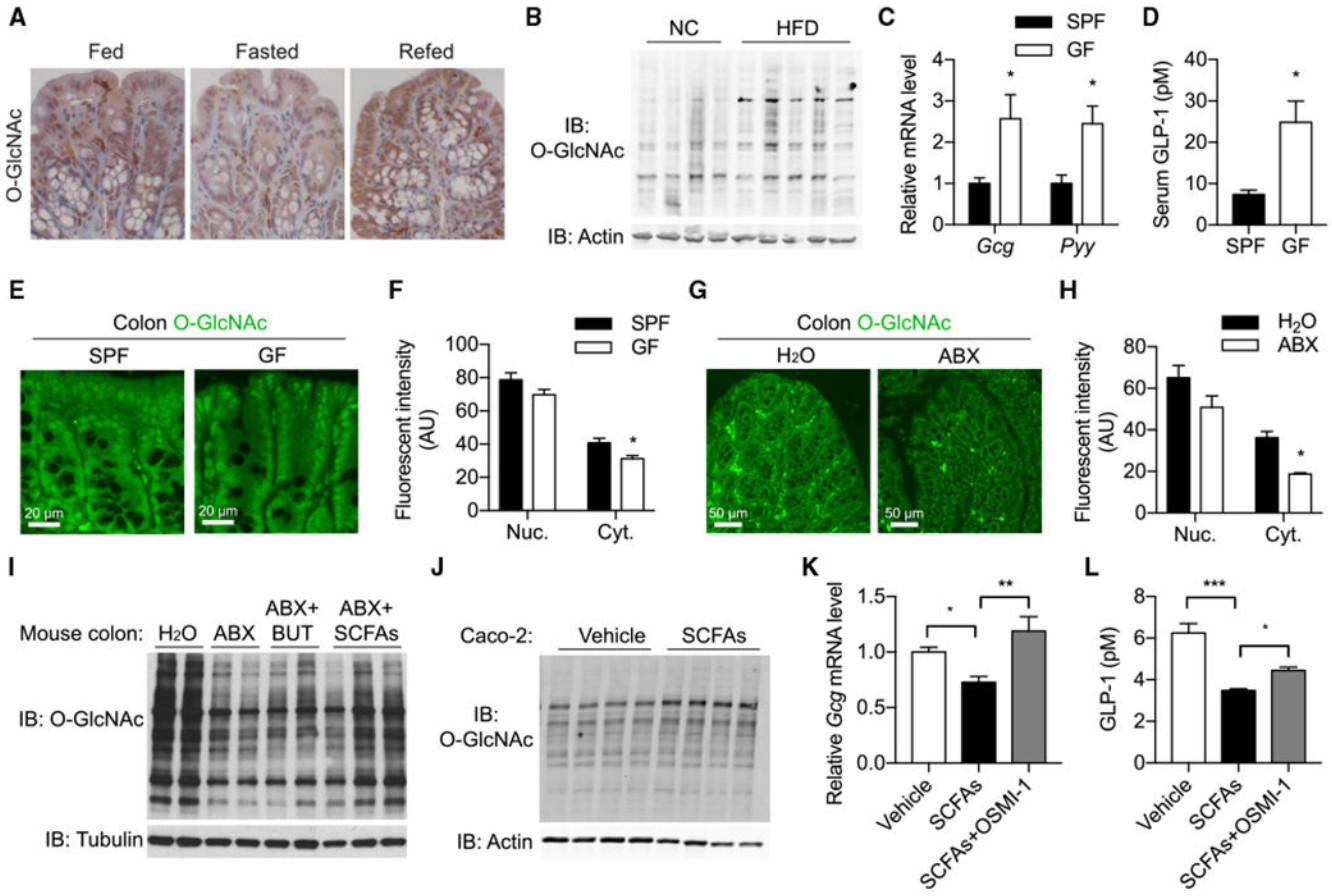

Figure 6. Regulation of L Cells and Protein O-GlcNAcylation by Gut Microbiota and Diet

(A) Representative images of O-GlcNAc immunohistochemistry of the colon from *ad-libitum-fed,* overnight-fasted, and 4-h-refed mice (n = 3).

(B) Immunoblotting of global protein O-GlcNAcylation in the colon of mice fed normal chow (NC; n = 4) or a high-fat diet (HFD; n = 5) for 2 months.

(C) Expression of the *Gcg* and *Pyy* genes in isolated colonic epithelial cells from 2-month-old SPF and GF mice (n = 5).

(D) GLP-1 levels in the serum of 2-month-old SPF and GF mice (n = 6), determined by ELISA.

(E and F) Representative images (E) and quantification (F) of O-GlcNAc immunostaining of the colon from 2-month-old SPF and GF mice (n = 5).

(G and H) Representative images (G) and quantification (H) of O-GlcNAc immunostaining of the colon from 2-month-old mice gavaged with H_2O or antibiotics (ABX) for 2 weeks (n = 6).

(I) Four-month-old mice were treated with saline or ABX for 1 week, followed by 2 doses (24 h and 4 h before sacrifice) of sodium butyrate (BUT) or SCFAs (3 g/kg body weight). Colon protein was extracted for immunoblotting with an anti-O-GlcNAc antibody.

(J) Caco-2 cells were serum-starved overnight, treated with SCFAs (8 μM each) for 24 h, and subjected to O-GlcNAc immunoblotting.

(K and L) Ileal organoids were treated with SCFAs and OSMI-1, as indicated, for 2 days. *Gcg* gene levels (K, n = 5–7) and GLP-1 secretion (L, n = 4–5) were determined. Data are represented as mean ± SEM. *p < 0.05, **p < 0.01, ***p < 0.001 by two-tailed unpaired Student's t test (C, D, F, and H) or one-way ANOVA with post hoc Dunnett's (K and L) test.

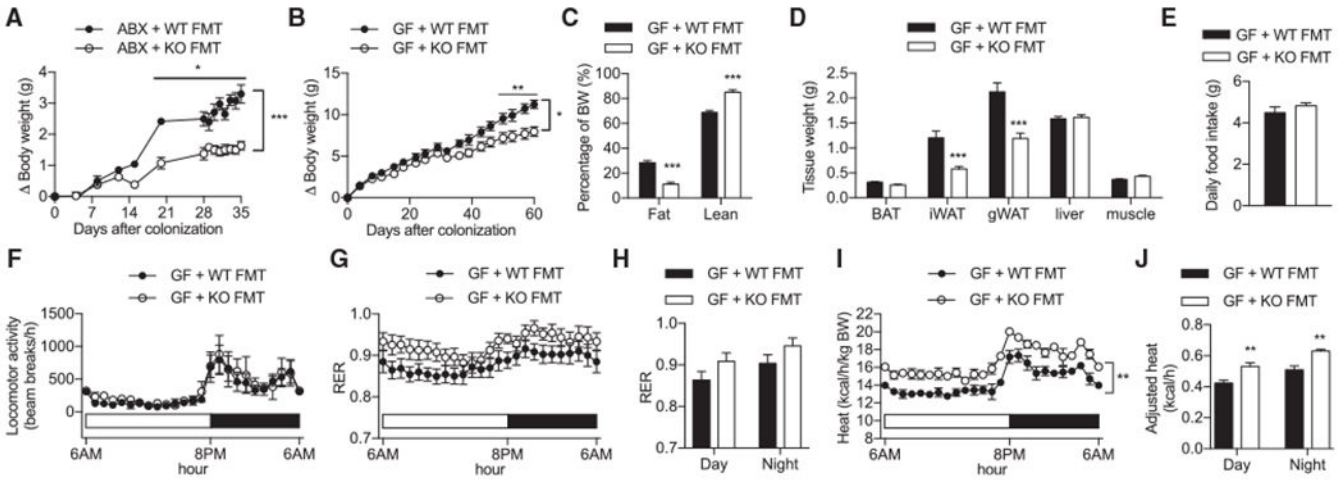

Figure 7. Gut Microbiota in *Vil-Ogt* KO Mice Promotes Metabolic Health

(A) 10-week-old C57BL/6 male mice were subjected to ABX gavage for 2 weeks to deplete gut microbiota and then received FMT (on days 0 and 8) from wild-type (WT) or *Vil-Ogt* KO mice. Body weight gain was monitored for 5 weeks (n = 10).

(B) Changes in body weight of 10-week-old GF male mice receiving FMT (on days 0 and 14) from WT or *Vil-Ogt* KO mice (n = 5).

(C) Body composition analysis showing percentages of fat and lean mass in mice 2 months after FMT (n = 5).

(D) Weight of intrascapular brown adipose tissue (BAT), inguinal WAT (iWAT), gonadal WAT (gWAT), liver, and quadriceps muscle in mice was determined 15 weeks after FMT (n = 5).

(E) Average daily food intake of FMT mice over 15 days (10–11 weeks after FMT, n = 5).

(F and J) Metabolic cage study of FMT mice (2 months after FMT, n = 5) showing daily locomotor activity (F), circadian RER (G), average RER during day and night (H), heat production normalized to body weight (I), and body weight-adjusted heat production (J) using ANCOVA.

Data are represented as mean –SEM. *p < 0.05, **p < 0.01, ***p < 0.001 by two-tailed unpaired Student's t test (C, D) or two-way ANOVA with post hoc Sidak's test (A, B, H, and J).

KEY RESOURCES TABLE

REAGENT or RESOURCE	SOURCE	IDENTIFIER
Antibodies		
Anti-O-GlcNAc antibody	Abcam	Cat# ab2739; RRID: AB_303264
Anti-GLP-1 antibody	Abcam	Cat# ab22625; RRID: AB_447206
Anti-ChgA antibody	Protein tech	Cat# 10529-1-AP; RRID: AB_2081122
Anti-PYY antibody	Cell Signaling Technology	Cat# 24895; RRID: AB_2798887
Anti-HA tag antibody	Cell Signaling Technology	Cat# 3724S; RRID: AB_1549585
Anti-OGT antibody	Cell Signaling Technology	Cat# 24083; RRID: AB_2716710
Anti-β-Actin antibody	Millipore Sigma	Cat# A5441; RRID: AB_476744
Anti-Flag M2 antibody	Millipore Sigma	Cat# F3165; RRID: AB_259529
Anti-Tubulin antibody	Santa Cruz	Cat# SC-8035; RRID: AB_628408
IRDye® 800CW Goat anti-Rat IgG Secondary Antibody	Li-Cor	Cat# 925-32219; RRID: AB_2721932
IRDye® 680RD Goat anti-Mouse IgG Secondary Antibody	LI-Cor	Cat# 926-68070; RRID: AB_10956588
Alexa Fluor 488 Donkey anti-Mouse Secondary Antibody	Invitrogen	Cat# R37114; RRID: AB_2556542
Alexa Fluor 488 Donkey anti-Rabbit Secondary Antibody	Invitrogen	Cat# R37118; RRID: AB_2556546
Chemicals, Peptides, and Recombinant Proteins		
Anti-FLAG® M2 Affinity Gel	Millipore Sigma	A2220
TRIzol reagent	Invitrogen	Cat# 15596018
iTaq Universal SYBR Green Supermix	Bio-Rad	Cat# 172-5124
RIPA buffer	Millipore Sigma	Cat# 20-188
Trypan blue solution	Millipore Sigma	Cat# 501613349
Matrigel	Corning	354230
Advanced DMEM/F12	Thermo Scientific	Cat# 12634-010
EGF	Peprotech	CaN/At # AF-100-15
Noggin	Peprotech	Cat# 250-38-100ug
R-spondin 1 conditioned medium	In-house production	N/A
Y-27632	Millipore Sigma	Cat# Y0503
HEPES	Thermo Scientific	Cat # 15630-56
Glutamax	Thermo Scientific	Cat # 35050-038
Penicillin/Streptomycin	Thermo Scientific	Cat # 15140-122
B-27 supplement (50X)	GIBCO	Cat # 17504-044
N2 supplement (100 X)	GIBCO	Cat # 17502-048
PBS	Corning	Cat # 21040CV
Vectashield Mounting Medium with DAPI	Vector Laboratories	Cat # H-1500
Insulin	Millipore Sigma	Cat# 91077C
Ampicillin Sodium Salt	Teknova	Cat# A9510
Gentamicin Sulfate	Teknova	Cat# G3610
Metronidazole	Spectrum	Cat# M1511

REAGENT or RESOURCE	SOURCE	IDENTIFIER
Neomycin Sulfate	Amresco	Cat# 0558
Vancomycin	VWR	Cat# 0990-5G
Sodium butyrate	Millipore Sigma	Cat# ARK2161
Sodium acetate	Millipore Sigma	Cat# S1429
Sodium propionate	Millipore Sigma	Cat# P5436
AS1842856	Calbiochem	Cat# 344355
6-Ac-CAS	GlycoSyn	Cat# FC-002
PUGNAc	Toronto Research Chemicals	Cat# A157250
OSMI-1	Millipore Sigma	Cat# SML1621
FITC-Dextran	Millipore Sigma	Cat# FD4
Lipofectamine 2000 Transfection Reagent	Invitrogen	Cat# 11668019
FuGENE® HD Transfection Reagent	Promega	Cat# E2311
Critical Commercial Assays		
Histostain-Plus 3rd Gen IHC Detection Kit	Life technologies	Cat# 859073
Rat/Mouse Insulin ELISA kit	Millipore Sigma	Cat# EZRMI-13K
Glucagon Like Peptide-1 (Active) ELISA kit	Millipore Sigma	Cat# EGLP-35K
PowerFecal DNA Isolation Kit	Mo Bio	Cat# 12830-50
Deposited Data		
16S sequencing	This paper	BioProject ID: PRJNA644017
Experimental Models: Cell Lines		
Human: HepG2	ATCC	HB-8065
Human: Caco-2	ATCC; share by Dr. Daniel A. Vallera	HTB-37
R-spondin stable cell line	from Dr. Noah Shroyer	N/A
Experimental Models: Organisms/Strains		
Mouse: Ogt-floxed mice	Jackson Laboratory	004860
Mouse: Rosa26-rOGT-floxed mice	Yang et al., 2020	N/A
Mouse: Villin-Cre	Jackson Laboratory	# 004586
Mouse: Neurog3-Cre mice	Jackson Laboratory	# 006333
Mouse: Vil-Ogt KO mice	This paper	N/A
Mouse: Ngn3-Ogt KO mice	This paper	N/A
Mouse: Vil-rOGTTg mice	This paper	N/A
Mouse: SPF C57BL/6 mice	Taconic Biosciences	B6-M MPF
Mouse: Germ-free C57BL/6 mice	Taconic Biosciences	B6-M GF
Oligonucleotides		
Table S2	This paper	N/A
Recombinant DNA		
Myc-hOGT plasmid	Chen et al., 2013	N/A
Ngn3-luc plasmid	This paper	N/A
IRE-luc plasmid	This paper	N/A

REAGENT or RESOURCE	SOURCE	IDENTIFIER
pCMV6-mNgn3-Myc-DDK	Origene	Cat# MR212139
pCMV-FOXO1	Addgene	Cat# 12148
pCMV-FOXO-4A	This paper	N/A
β-galactosidase	Ruan et al., 2012	N/A
Renilla-luciferase	Wang et al., 2018	N/A
Software and Algorithms		
Graphpad Prism 7	https://www.graphpad.com	N/A
FIJI	https://imagej.net/Fiji	N/A
Other		
Contour glucometer	Bayer	Cat# 9545C
Blood glucose test strips	Bayer	Cat# 7097C